Regulation of neuronal mRNA splicing and Tau isoform ratio by ATXN3 through deubiquitylation of splicing factors

RUNNING TITLE: Neuronal splicing regulation by ATXN3

Andreia Neves-Carvalho[1,2], Sara Duarte-Silva[1,2], Joana Silva[1,2], Bruno Almeida[1,2], Sasja Heetveld[3], Ioannis Sotiropoulos[1,2], Peter Heutink[3], Ka Wan Li[4] and Patrícia Maciel[1,2*]

[1] Life and Health Sciences Research Institute (ICVS), School of Medicine, University of Minho, Braga, Portugal

[2] ICVS/3B's – PT Government Associate Laboratory, Braga/Guimarães, Portugal

[3] German Center for Neurodegenerative Diseases (DZNE), 72076 Tübingen, Germany

[4] CNCR, Amsterdam Neuroscience, Vrije Universiteit, Amsterdam, The Netherlands

CORRESPONDING AUTHOR:
Patrícia Maciel, PhD
Associate Professor
School of Medicine
University of Minho
Braga, Portugal
Telephone: 351-253-604824
Fax: 351-253-604820
E-mail: pmaciel@med.uminho.pt
ORCID ID: 0000-0002-4151-6885

FUNDING

This work has been funded by FEDER funds, through the Competitiveness Factors Operational Programme (COMPETE), and by National funds, through the Foundation for Science and Technology (FCT), under the scope of the project POCI-01-0145-FEDER-007038 and through the project POCI-01-0145-FEDER-016818 (PTDC/NEU-NMC/3648/2014) and fellowships [SFRH/BD/51059/2009 to A. N-C, SFRH/BPD/110728/2015 to B.A, SFRH/BD/78388/2011 to S.D-S, SFRH/BD/88932/2012 to J.M.S and IF/01799/2013 to I.S.

ABSTRACT

The ubiquitylation/deubiquitylation balance in cells is maintained by Deubiquitylating enzymes, including ATXN3. The precise role of this protein, mutated in SCA3, remains elusive, as few substrates for its deubiquitylating activity were identified. Therefore, we characterized the ubiquitome of neuronal cells lacking ATXN3, and found altered polyubiquitylation in a large proportion of proteins involved in RNA metabolism, including splicing factors. Using transcriptomic analysis and reporter minigenes we confirmed that splicing was globally altered in these cells. Among the targets with altered splicing was SRSF7 (9G8), a key regulator of MAPT (Tau) exon 10 splicing. Loss-of-function of ATXN3 led to a deregulation of MAPT exon 10 splicing resulting in a decreased 4R/3R-Tau ratio. Similar alterations were found in the brain of a SCA3 mouse and humans, pointing to a relevant role of this mechanism in SCA3, and establishing a previously unsuspected link between two key proteins involved in different neurodegenerative disorders.

Ataxin-3/ Neurodegeneration/ Serine-Arginine rich splicing factor 7 (SRSF7 or 9G8)/ Splicing/ Ubiquitylation

INTRODUCTION

Ubiquitin signaling is now recognized as a fundamental molecular mechanism tightly regulating a broad range of intracellular events [1-3]. Ubiquitylation is a highly dynamic biochemical modification in which an ubiquitin (Ub) moiety is attached to a protein. This process is catalyzed by the sequential actions of Ub-activating enzyme (E1), Ub-conjugating enzymes (E2) and Ub-protein ligases (E3) that bind Ub to different lysine (K) residues in the substrate, resulting in mono or poly Ub chains (Reviewed in [4]). Ubiquitylated substrates are then recognized by proteins containing ubiquitin binding domains and directed to different fates. For example, K48 usually targets proteins for proteasomal degradation [4], while K63-linked polyUb regulates protein activation, subcellular localization or degradation in the lysosome (autophagy) and is known to be relevant for DNA repair (Reviewed in [5]). Ubiquitylation and proteolysis by the Ubiquitin-proteasome pathway (UPP) are now well-known as important mechanisms in the nervous system as this proteolytic pathway is known to degrade misfolded or short-lived regulatory proteins (Reviewed in [1,6]). Impairment of the UPP has been connected to several neurodegenerative diseases such as Alzheimer's (Reviewed in [7]), Parkinson's (Reviewed in [8]) and Hungtington's (Reviewed in [9]) diseases. Like most post-transcriptional modifications, ubiquitylation is a reversible signal and is counterbalanced by deubiquitylating (DUB) enzymes, which remove Ub units and play an important role in the modulation of proteins by the proteasome as well as the autophagic pathway [10-12], and in Ub signaling in general. Several pieces of evidence have suggested that Ub may also regulate splicing: (i) Ub and Ub-

83 like proteins have been shown to copurify with splicing complexes [13,14], (ii)
84 ubiquitylated splicing factors have been identified in proteomic screenings [15,16]
85 and (iii) several functional domains related to Ub pathway have been
86 identified in important spliceosome proteins, such as Jab1/MPN domain of the
87 essential U5 SnRNP component Prp8 [17-20]. Thus, the action of DUBs has a
88 major impact on the ubiquitylated proteome (also known as ubiquitome).
89 Ataxin-3 (ATXN3) is a protein with DUB activity known to be involved in
90 Spinocerebellar ataxia type 3 (SCA3)/ Machado Joseph disease (MJD), a
91 neurodegenerative disorder of adult onset caused by the expansion of a
92 polyglutamine (polyQ) tract in this protein. Interestingly, in addition to being
93 involved in global protein quality control responses [21,22], normal ATXN3
94 appears to participate in cell adhesion and in the organization of cytoskeleton
95 network [23-26], to be involved in transcriptional regulation and DNA repair [27-29],
96 and to be required for neuronal differentiation [25]. Nevertheless, the relative
97 relevance of these functions and the physiological role of this highly
98 conserved but genetically non-essential protein remains to be clarified and its
99 substrates are also not well characterized, particularly in neurons. Given the
100 known relevance of UPP in neuronal function and its link to nervous system
101 diseases, we sought to clarify the precise role of ATXN3. To identify potential
102 candidates for the DUB activity of this protein, we characterized changes in
103 the ubiquitome of neuronal cells lacking ATXN3 ($ATXN3^{shRNA}$ cells) by mass-
104 spectrometry, and identified for the first time a role for ATXN3 in RNA
105 metabolism. We found a global perturbation of splicing in the absence of this
106 protein, among which a mis-splicing of tau exon 10 which perturbs the 4R/3R

107 tau ratio, a mechanism that may contribute for SCA3 pathogenesis, and links
108 two key proteins involved in different neurodegenerative disorders.
109
110 **RESULTS**
111
112 **Changes in the ubiquitome of cells lacking ATXN3 suggest a link to RNA**
113 **metabolism**
114 With the goal of identifying substrates of the DUB activity in neuronal cells, we
115 searched for changes in the ubiquitome of neuronally differentiated SH-SY5Y
116 cells lacking ATXN3 ($ATXN3^{shRNA}$ cells - Figure EV1A-B)[25], taking advantage
117 of a recently developed methodology that combines capture of the whole
118 spectrum of polyubiquitylated proteins in a cell extract using an enrichment by
119 Tandem Binding Ubiquitin Entities (TUBEs) followed by mass spectrometry
120 analysis (TUBEs-LC-MS/MS) [30]. Figure 1A summarizes the steps followed for
121 the purification and identification of the polyubiquitylated proteins in
122 $ATXN3^{shRNA}$ and scrambled control shRNA (SCR^{shRNA}) cells. The integration
123 of the data and the comparison between the proteins identified in $ATXN3^{shRNA}$
124 versus SCR^{shRNA} cells resulted in a list of proteins with altered
125 polyubiquitylation in cells lacking ATXN3; among these are potential targets of
126 the DUB activity of ATXN3, i.e., putative ATXN3 substrates. In each pulldown
127 experiment, around 1200-1300 proteins were identified. When the results of
128 all the independent experiments were merged, we observed that many of
129 these proteins were only sporadically detected across the different
130 experiments; for the remaining analysis, these proteins were excluded,
131 reducing the list to 615 consistently identified proteins. From these, 193

132 proteins showed altered levels in the polyubiquitylated fraction in ATXN3^{shRNA}
133 cells when compared to the SCR^{shRNA} controls ($p<0.05$) (Table EV1). The
134 majority of these polyubiquitylated proteins were either not detected (44.04%)
135 or showed decreased levels (24.35%) in ATXN3^{shRNA} cells when compared to
136 the controls. These proteins can be grouped into 10 functional networks, the
137 most representative being related to: (i) Gene expression, DNA replication,
138 recombination and repair (17.7%), (ii) RNA post-transcriptional modification
139 (13.3%), (iii) Molecular transport, RNA trafficking (10.8%), (iv) Cell death and
140 survival (8.9%) and (v) Organ morphology (8.9%) (Figure 1B). The fact that a
141 significant proportion of the proteins with altered polyubiquitylation in
142 ATXN3^{shRNA} cells are RNA metabolism-related proteins, around 8% of them
143 being splicing factors (Table 1), suggested to us that ATXN3 could be playing
144 a role in mRNA splicing, a previously undescribed role for this DUB.
145
146 **Cells lacking ATXN3 show global perturbation of splicing**
147 We hypothesized that absence of ATXN3 could lead to a deregulation of the
148 pre-mRNA splicing process. To address this, we used three hybrid minigene
149 reporter plasmids: the pyPY minigene, representing splicing events with
150 alternative competing 3' acceptor sites/splice sites, the AdML minigene,
151 representing constitutive/strong splicing events, and the α-globin minigene, for
152 which the alternative splicing (exon skipping) is indicative of the performance
153 of regulatory splicing factors such as hnRNP and SF proteins [31,32]. As shown
154 in Figure 2A-D, knockdown of ATXN3 significantly altered the processing of
155 the three splicing reporters, suggesting a general deregulation of splicing in
156 the absence of this protein. Interestingly, overexpression of a catalytically inert

157 version of ATXN3 in SH-SY5Y cells (ATXN3_C14A), previously shown to
158 have a dominant-negative effect [25] also yielded similar alterations (Figure 2E).
159 Consistent with a global deregulation of splicing in the absence of ATXN3,
160 microarray analysis (Figure 2F) using specific arrays containing additional
161 probes for exon/exon junctions, confirmed that 1993 genes (43%), from the
162 7450 differentially expressed probes in ATXN3^{shRNA} cells, presented
163 differentially regulated alternative splicing events (Table EV1). These genes
164 mainly encode components with function in protein degradation systems, cell
165 adhesion, axon guidance and various signaling pathways (Table EV2), the
166 majority of splicing events being decreased when compared to control cells
167 (Table EV3). The most affected alternative splicing event types were exon
168 cassette usage (34%), complex splicing (20%) and intron retention (15%)
169 (Figure 2G). Alternative terminal exon usage, which can be mechanistically
170 linked to alternative splicing, was also seen in 16% of the cases (Figure 2G).
171 Being a key mechanism in the regulation of gene expression, defects in these
172 regulatory processes may affect a multiplicity of cellular functions related to
173 disease.
174
175 **ATXN3 modulates SRSF7 degradation by the proteasome**
176 Interestingly, among the splicing factors with differential ubiquitylation was the
177 Arginine/Serine-Rich splicing factor SRSF7 (also known as 9G8), known to be
178 involved in the regulation of alternative splicing of the neurodegeneration-
179 related gene *MAPT* [33], encoding the Tau protein. As shown in Figure 3A-B,
180 we detected decreased levels of ubiquitylated forms of SRSF7 in cells lacking
181 ATXN3 (p=0.02), validating the data obtained with the proteomic analysis.

182 Consistent with the hypothesis that the differential ubiquitylation of SRSF7
183 can have an impact on its degradation, the steady state levels of total (Figure
184 3A-B) and nuclear (Figure 3C-D) SRSF7 were decreased in ATXN3^{shRNA} cells
185 as compared with the SCR^{shRNA} control cells (p=0.025 and p=0.001,
186 respectively). This suggests that SRSF7 is indeed being more degraded in the
187 absence of ATXN3, confirming that ATXN3 affects the expression of SRSF7
188 at the protein and not at the mRNA level (p=0.712) (Figure EV1C).
189 Based on the fact that SRSF7 was captured using Agarose-TUBEs that have
190 higher affinity for polyubiquitylated than for monoubiquitylated proteins [30] and
191 considering that ATXN3 is a DUB, we asked if ATXN3 could modify
192 ubiquitylation and regulate degradation of SRSF7 through the UPP.
193 Supporting this possibility, the levels of SRSF7 were significantly increased in
194 ATXN3^{shRNA} cells upon proteasome inhibition with MG132 p=0.0016) (Figure
195 3E-F). Additionally, we detected lower levels of polyubiquitylated SRSF7
196 presenting Ub-K48 linkages (Figure 3G), a type of Ub chain that usually
197 signals proteins for degradation through the UPP. Protein stability analysis
198 upon inhibition of protein synthesis by cicloheximide treatment showed a
199 decrease in the half-life of SRSF7 in ATXN3^{shRNA} cells (Figure 3H), suggesting
200 that ATXN3 normally acts to inhibit SRSF7 degradation in neurons. In order
201 for ATXN3 to modify the ubiquitylation and stability of SRSF7, the two proteins
202 need to interact. Co-immunoprecipitation using protein extracts from
203 differentiated neuron-like SH-SY5Y cells confirmed that an interaction
204 between ATXN3 and SRSF7 occurs in these cells (Figure 3I). This interaction
205 was further confirmed in live cells by the Protein Ligation Assay (Figure 3J,

206 Figure EV1E). Globally, our data are compatible with the hypothesis of
207 SRSF7 being a substrate of the DUB activity of ATXN3 in neurons.
208
209 **Tau splicing is deregulated in the absence of ATXN3**
210 Given that one of the splicing factors showing differential ubiquitylation was
211 SRSF7, we next analyzed mRNA levels of Tau isoforms in ATXN3^{shRNA} cells
212 to assess the functional impact of the reduction of this splicing factor in Tau
213 splicing. We found a significant decrease in the transcript levels of 4R-Tau
214 isoform ($p=7.4x10^{-11}$) (Figure 4A), but no alteration of the 3R-Tau isoform
215 ($p=0.270$) in ATXN3^{shRNA} cells as compared with SCR^{shRNA} control cells
216 (Figure 4B), leading to an altered 4R/3R-Tau ratio ($p=2,98x10^{-6}$) and
217 decreased total tau levels ($p=1.92x10^{-4}$), both in ATXN3^{shRNA} cells (Figure 4D)
218 as well as in cultured primary cerebellar neurons ($p=3.23x10^{-9}$) in which
219 ATXN3 expression was silenced by shRNA (Figure EV1D, Figure 4E-H).
220 Consistently, catalytically inactive (Dominant negative) ATXN3 expression
221 also led to alterations in tau expression and in the isoform ratio similar to
222 those seen in cells with silenced ATXN3: decreased expression of 4R-Tau
223 ($p=1.1x10^{-5}$) (Figure 4I), no alterations on the 3R-Tau isoform (Figure 4J), and
224 consequentially a decreased 4R/3R-Tau ratio ($p=0.0088$) (Figure 4K) and
225 decreased levels of total Tau ($p=1.20x10^{-6}$) (Figure 4L). To explore the
226 functional consequences of this reduction in 4R-Tau levels, we performed a
227 morphometric analysis of these cells. ATXN3^{shRNA} cultures presented a
228 decreased expression of βIII-tubulin and a decreased average length of the
229 neuritis as compared with the SCR^{shRNA} controls, which correlates with a more
230 immature stage of neuronal differentiation (Figure 4M-N).

231

232 **Decreased SRSF7 expression and Tau splicing perturbation in SCA3**
233 **models and patients**

234 To determine if the presence of an expanded polyglutamine (polyQ) tract
235 within ATXN3 would lead to an alteration in this newly identified physiological
236 function, we analyzed a SH-SY5Y cell line expressing a version of ATXN3
237 bearing 83 glutamines (ATXN3_83Q), and found a globally decreased
238 efficiency of splicing (Figure 5A). We next asked whether the presence of the
239 polyQ tract could also impact *MAPT* mRNA splicing regulation, altering the
240 4R/3R-Tau ratio. Interestingly, expression of ATXN3_83Q lead to similar
241 changes in the expression of tau isoforms as observed in cells lacking ATXN3
242 or expressing a catalytic mutant version of this protein: i) decreased
243 expression of 4R-Tau isoform ($p=6.6x10^{-5}$) (Figure 5B), ii) no alterations on
244 the 3R-Tau isoform (Figure 5C), iii) a decrease of the 4R/3R-Tau ratio
245 ($p=2.4x10^{-4}$) (Figure 5D), and (iv) a decrease in the levels of total Tau
246 ($p=7.6x10^{-6}$) (Figure 5E).. Of notice, the overexpression of the wild type
247 ATXN3 (ATXN3_28Q) also caused some (albeit less important) degree of
248 perturbation (Figure 5 A-E), pointing to the importance of a tight regulation of
249 ATXN3 dosage in neurons.

250 Tau splicing was also analyzed in SCA3 mouse model (CMVMJD135) that
251 reproduces key features of the disease [34]. A decreased expression of the 4R-
252 Tau isoform was seen in the brainstem (affected brain region) of CMVMJD135
253 mice (Tg) ($p=7x10^{-5}$) comparing with the Wild type (Wt) controls (Figure 5F),
254 with no alterations of the 3R-Tau isoform expression (p=0.84) (Figure 5G),
255 leading to an altered 4R/3R-Tau ratio ($p=1.2x10^{-3}$) (Figure 5H) and decreased

levels of total Tau ($p=1.1x10^{-8}$) (Figure 5I). In addition, SRSF7 protein levels were also reduced in the brainstem (p=0.0093), spinal cord (p=0.0014) and to a lesser extent in the cerebellum (p=0.1138) (disease-affected brain areas) of Tg mice as compared with the Wt littermate controls (Figure 5J-L, respectively), but no alterations at the mRNA level were detected (Figure EV1F). This indicates that the impact of ATXN3 on tau splicing through the control of SRSF7 levels is also occurring in SCA3 and is corroborated by the decreased levels of SRSF7 protein present in the brains of SCA3 patients as compared with healthy controls (Figure 5M). To explore the functional consequences of this reduction in 4R-Tau levels, an isoform of Tau associated with mature neurons and synaptic function, we performed a morphometric analysis of neurons in this brain region. A decreased mean neurite length (p=0.0189) (Figure 5N-O) and a decrease in complexity of the dendritic trees (p=0.0004) (Figure O, P) were observed in neurons from the Medial vestibular nuclei in the Brainstem.

Altogether, these results suggest that the functional interaction of ATXN3 with SRSF7 and its impact on molecular mechanisms regulating tau splicing in neurons may be relevant in the pathogenesis of SCA3.

DISCUSSION

Ubiquitylation is a post-translational modification that controls several aspects of neuronal function by regulating protein abundance. Disruption of this signaling pathway has been described in neurodegenerative diseases. Indeed, since many of these diseases exhibit ubiquitylated protein aggregates, loss of ubiquitin homeostasis may be an important contributor for

281 disease. Considering the importance of DUB enzymes in maintaining the
282 ubiquitylation balance, we focused on the characterization of the ubiquitome
283 of neuronal cells lacking ATXN3 [25]. Using TUBEs, that enable the pulldown of
284 polyubiquitylated proteins without further genetic manipulation or inhibition of
285 the proteasome [30] in combination with LC-MS/MS, we were able to
286 consistently identify 615 proteins per condition, a yield comparable to those
287 described in other studies [35,36]. Among the proteins identified, approximately
288 one third presented altered levels of polyubiquitylation in ATXN3^{shRNA} cells.
289 Curiously, the majority of these proteins presented decreased levels in the
290 polyubiquitin-enriched fraction signal, suggesting that normally ATXN3 might
291 be preventing their degradation, for instance by editing the substrate's
292 ubiquitin chains, as we observed before for ITGA5 [24,25]. Therefore, when
293 ATXN3 is silenced, the polyubiquitin signal is not removed, which may result
294 in an increased degradation of the targeted proteins. The fact that a significant
295 proportion of the proteins with altered polyubiquitylation levels in ATXN3^{shRNA}
296 cells were splicing factors and proteins involved in RNA processing, is
297 suggestive of ATXN3 playing a role in the pre-mRNA splicing process in
298 neuronal cells. This process is particularly important in generating diversity
299 and specificity in the central nervous system, which requires a wide protein
300 repertoire to generate its highly specialized and adaptable neuronal circuits [37].
301 Given the importance of RNA processing for neuronal function, it comes as no
302 surprise that altered RNA processing is a contributing factor to the
303 pathogenesis of multiple neurodegenerative diseases [38-42]. Disruption of
304 alternative slipicing (AS) regulation, resulting from mutations or abnormal
305 expression of RNA-binding proteins, can lead to an imbalance or an

306 inappropriate expression pattern of key protein isoforms, with profound
307 consequences on cellular and organismal physiology. Indeed, the relative
308 concentration of splicing factors and hnRNPs, which may be regulated by the
309 Ub pathway, has been shown to regulate AS [43]. For example, it was shown
310 that the abundance of several splicing factors is differentially affected by
311 proteasome inhibition, and abnormal levels of these regulatory proteins were
312 associated with a different AS pattern [44]. Another study showed that the
313 splicing factor SRSF5 is targeted to proteasomal degradation as the cells
314 undergo terminal differentiation [45]. Consistently, assessed general splicing
315 efficacy was decreased in cells depleted of ATXN3, as shown using artificial
316 reporter minigenes, further supporting the involvement of ATXN3 in the
317 regulation of the splicing process. Additionally, genome wide microarray
318 analysis of endogenous splicing events confirmed that absence of ATXN3
319 leads to a dramatic alteration in the splicing pattern of a large number of
320 genes in neuronal cells, including genes related to protein degradation,
321 adhesion, axon guidance and signaling pathways. This is consistent with our
322 previous findings showing that absence of ATXN3 leads to an impairment in
323 neuronal differentiation and adhesion [25], and affects the degradation of
324 several target proteins [23-25]. Significantly, a portion of the predicted splicing
325 regulators of these genes with altered splicing in cells lacking ATXN3 were
326 found to have altered levels of polyubiquitylation in our proteomic analysis, the
327 majority of them being Serine/Arginine (SR) – rich phosphoproteins. Proteins
328 of the SR family are key players in the control of AS, regulating the selection
329 of alternative sites [46,47]. The fact that SRSF7 (9G8), one of those proteins and
330 a key regulator of MAPT (tau) exon 10 splicing [48,49], was captured using the

331 Agarose-TUBEs, which have high affinity for polyubiquitin chains [30],
332 suggested that this splicing factor is polyubiquitylated, and thus might be
333 degraded through the UPP. Indeed, while it has been described that the
334 mature human neurons express approximately equal levels of 4R and 3R-Tau
335 isoforms [50,51], whose expression is developmentally controlled and finely-
336 tuned, we found that loss of function of ATXN3 disrupts this balance in
337 neuronal cells leading to a decreased 4R/3R-Tau ratio, that coincides with
338 (and may be caused by) decreased levels of SRSF7. Very recent works have
339 shown imbalanced expression in 3R and 4R-Tau, namely a decreased
340 expression of the 4R isoform as here observed, in the brain of a mouse model
341 of Down syndrome, but also in human AD and PD patients [52-54], strengthening
342 the idea that a faulty tau exon 10 splicing might be contributing for the
343 pathogenesis of several neurodegenerative diseases. In addition, the
344 decreased levels of the 4R-Tau isoform presented by ATXN3^{shRNA} cells, also
345 correlate with the immature phenotype of these cells, that we previously
346 described [25]. Indeed Conejero-Godberg and colleagues also assessed the
347 transcriptional profiles related to 3R and 4R-Tau splice variants, revealing that
348 a cluster of genes related to neuronal cell morphology and outgrowth of
349 neurites is upregulated in the presence of 4R isoforms, while genes related to
350 cellular growth and proliferation were downregulated [55]. This is in agreement
351 with previous work from Sennvik's team establishing a role for 4R-Tau
352 isoforms in promoting neuronal differentiation [56]. Taking into account that loss
353 of function of ATXN3 leads to a deregulation in the amount of SRSF7, at the
354 protein level but not RNA level, we hypothesized that this splicing factor could
355 be a substrate of the DUB activity of ATXN3, which could be modulating its

356 degradation. In line with that, we confirmed that ATXN3 interacts closely with
357 SRSF7 in neuronal cells, suggesting that these proteins are molecular
358 partners in such cells, and establishing a functional link between two key
359 proteins involved in different neurodegenerative diseases. Trying to explore if
360 this interaction could be indicative that ATXN3 is modulating the degradation
361 of SRSF7 through the proteasome, we measured the levels of this protein
362 upon proteasome inhibition; as expected, we saw an accumulation of SRSF7
363 when the proteasome was inhibited. Interestingly, we also found a decreased
364 4R/3R-Tau ratio, as well as decreased protein levels of SRSF7, both in cells
365 expressing the mutant protein, in affected brain regions of our mouse model
366 for the disease, at an age when the transgenic animals display an overt
367 phenotype resembling behavioral and pathological characteristics present in
368 human patients [34]. This suggests that the mis-splicing of tau may be
369 contributing to SCA3 pathogenesis, as it does to other neurodegenerative
370 diseases. Considering that we observed a similar phenomenon using cells
371 lacking ATXN3 and cells expressing a catalytic inactive mutant form of the
372 protein, it is reasonable to think that the DUB activity of ATXN3 is important in
373 this cellular process and that the polyglutamine expansion might cause a
374 partial loss of this normal function of the protein (even in presence of 50% of
375 the wild type protein), perhaps through a dominant negative mechanism, thus
376 contributing to SCA3 pathogenesis. Indeed, Winborn and co-workers
377 demonstrated that while expression of ataxin-3 with a non-pathogenic polyQ
378 tract leads to a reduction in total ubiquitylated protein levels in cells, this
379 reduction is not observed upon overexpression of an expanded ataxin-3,
380 which may reflect inefficient deubiquitylation of cellular proteins, pointing to an

381 overall loss of function [57]. Overall, our data suggest that ATXN3 is involved in
382 splicing regulation through the modulation of the ubiquitylation of splicing
383 factors. This regulatory role may be mediated through the DUB activity of
384 ATXN3 by modulating activation, degradation and/or subcellular localization of
385 the splicing factors, or may be an indirect result of the modulation of E3
386 ligases specific for these targets.

387 Recently, several pieces of evidence coming from the use of technologies
388 such as exon arrays and RNA-Seq suggested an association between
389 perturbation of AS and several neurodegenerative diseases including
390 Alzheimer's disease, Huntington's disease, Pick's disease, Spinal Muscular
391 atrophy and Amyotrophic Lateral Sclerosis [58-60]. Importantly, several ataxia-
392 causing proteins have been described to interact with splicing factors [61]. Also,
393 expression of mutant ATXN3 bearing an expanded polyglutamine tract was
394 previously shown to alter the ability of the subnuclear domains known as Cajal
395 bodies to efficiently participate in small nuclear ribonucleoprotein (snRNP)
396 biogenesis pathway, and to reduce the efficacy of splicing reporter genes [62].
397 These findings lead us to propose that ATXN3 plays a role in splicing
398 regulation in neurons, a novel function for this protein, and that a perturbation
399 of this physiological function might contribute for SCA3 pathogenesis.

400

401 **MATERIALS AND METHODS**

402

403 **Cell lines and primary cultures**

404 *SH-SY5Y cell cultures:* SH-SY5Y human female neuroblastoma cell line
405 (ATCC number CRL-2266) was cultured in Dulbecco's modified eagle
406 medium: nutrient mixture (DMEM)/F-12 supplemented with 10% (v/v) fetal
407 bovine serum (FBS) (Biochrom), 2mM glutaMAX (Invitrogen), 100 U/mL
408 penicillin (Invitrogen), 100 µg/mL streptomycin (Invitrogen) and 25 ng/mL
409 puromycin (Sigma Aldrich). Medium was changed every 2 days. Cells were
410 transfected with a shRNA sequence targeting *ATXN3* or a scrambled shRNA
411 sequence as described elsewhere [25]. Differentiation of stably infected cell
412 lines was induced by 0.1 µM all-trans-retinoic acid (RA) (Sigma Aldrich) in
413 opti-MEM (Invitrogen) supplemented with 0.5% FBS for 7 days. Medium was
414 replaced every 2 days. *Primary cultures of cerebellum:* cerebellar neuron
415 cultures were prepared from P7 Wistar rats. Briefly, upon dissection, cerebella
416 were submitted to a trypsin-based enzymatic digestion followed by
417 mechanical dissociation. Isolated cells were plated on poly-d-lysine (Sigma
418 Aldrich) and lysine (Sigma Aldrich) pre-coated 6-well plates at a density of
419 $1.25x10^6$ cells/mL using Neurobasal A (Invitrogen) supplemented with 1x B27
420 (Invitrogen), 0.1 mg/mL Kanamycin (Invitrogen), 1 mM Glutamax I (Invitrogen)
421 and 10 ng/mL bFGF (Invitrogen) for 7 days. Half of the medium was changed
422 every 4 days.
423
424 **Mice**
425 Female CMVMJD135 (background C57BL/6) mice were used in the study.
426 Transgenic (Tg) and wild-type (Wt) littermates were housed at weaning in
427 groups of 5 animals in filter-topped polysulfone cages 267x207x140 mm (370
428 cm^2 floor area) (Tecniplast), with corncob bedding (Scobis Due, Mucedola

429 SRL) in a conventional animal facility. The mice were genotyped at weaning
430 by PCR, as we previously described [63]. All animals were maintained under
431 standard laboratory conditions: an artificial 12 h light/dark cycle (lights on from
432 8:00 to 20:00 h), with an ambient temperature of 21±1ºC and a relative
433 humidity of 50-60%; the mice were given a standard diet (4RF25 during the
434 gestation and postnatal periods, and 4RF21 after weaning (Mucedola SRL)
435 and water *ad libitum*. Animal facilities and the people directly involved in
436 animal experiments were certified by the Portuguese regulatory entity –
437 Direcção Geral de Veterinária. Health monitoring was performed according to
438 FELASA guidelines[64], confirming the Specified Pathogen Free status of
439 sentinel animals maintained in the same animal room. Humane endpoints for
440 the experiment were defined (20% reduction of the body weight, inability to
441 reach food and water, presence of wounds in the body, dehydration). The
442 animals were euthanized at 45 weeks of age by decapitation, the brain
443 regions of interest were macro dissected and store at -80ºC until further
444 processing.
445
446 **Pulldown of polyubiquitylated proteins**
447 Cells treated with RA were lysed by sonication on ice in lysis buffer (50 mM
448 Tris-HCl pH 7.5, 0.15 M NaCl, 1mM EDTA, 1% NP-40, 10% Glycerol,
449 complete protease inhibitors (Roche) and 50 µM UB/UBl protease inhibitor
450 PR-619 (LifeSensors). After lysis, 2 mg of total protein extract was incubated
451 with 100 µL of pre-equilibrated Agarose-TUBEs (LifeSensors), overnight at
452 4ºC on a rocking platform. Sedimented beads were washed 3 times with
453 washing buffer (20 mM Tris pH 8.0, 0.15 M NaCl, 0.1% Tween-20) before

454 being eluted with 1x SDS sample buffer (62.5mM Tris-HCl pH 6.8, 10%
455 glycerol, 2% SDS, Bromophenol Blue). Eluted proteins were immediately
456 boiled at 98ºC for 15min and ran in a 10% SDS-PAGE gel. After incubation
457 with the FK2 anti-ubiquitin primary antibody (1:2000, Millipore) overnight at
458 4ºC, membranes were incubated with secondary antibody for 1 hour at room
459 temperature (anti-mouse, 1:10.000, Bio-Rad). Antibody binding was detected
460 by chemiluminescence (Clarity kit, Bio-Rad).
461
462 **Digestion of proteins from preparative 1D-PAGE gel**
463 The 1D PAGE LC-MS/MS approach was used for protein identification as
464 previously described [65]. Eluted proteins were separated using 1.5 mm and
465 10% SDS-PAGE gels. The quality of purification was controlled by Coomassie
466 Brilliant Blue g-250 (Sigma) staining before MS analysis. Gel image was
467 acquired the Gel Doc™ EZ system (Bio-rad). After Coomassie staining, all the
468 visible blue-stained protein spots were manually excised from the gel. The gel
469 pieces were destained overnight at room temperature using 50% acetonitrile
470 in 25 mM ammonium bicarbonate buffer, pH 8.5, and then dehydrated with
471 100% acetonitrile. The shrunken pieces were then re-swollen in 50 mM
472 ammonium bicarbonate buffer, dehydrated in 100% acetronitrile and dried in a
473 speedvac® concentrator (Savant) for 30 min. The gel pieces were rehydrated
474 in 60 µL of 20 µg/mL Trypsin (Promega) in 50 mM ammonium bicarbonate
475 solution and incubated for 2h at 55ºC. The gel pieces were then incubated
476 with 0.1% trifluoroacetic acid in 50% acetonitrile for 20 min at room
477 temperature in order to extract the remaining peptides from the gel. The
478 tryptic peptides were dried in a speedvac for 2 h.

479

480 **Liquid chromatography-tandem mass spectrometry (LC-MS/MS)**

481 After re-dissolution in 17 µL 0.1% acetic acid, samples were separated on a
482 capillary C18 column using a nano LC-ultra 1D plus HPLC system (Eksigent)
483 and analyzed on-line with an electrospray LTQ-Orbitrap Discovery mass
484 spectrometer (Thermo Fisher Scientific). MS/MS spectra were searched
485 against a human database (uniprot_sprot, 2010_01) with the ProteinPilot™
486 software (version 3.0; AB-sciex) using the Paragon™ algorithm (version
487 3.0.0.0 [66]) as the search engine. The detected protein threshold (unused
488 protscore (confidence)) in the software was set to 0.10 to achieve 20%
489 confidence and the proteins identified were grouped to minimize redundancy.
490 Peptides with "unused" values < 2 have low confidence and were excluded
491 from analysis. The "unused" value is defined in the handbook of ProteinPilot
492 as a sum of peptide scores from all the non-redundant peptides matched to a
493 protein. Peptides with confidence of ≥ 99% would have a peptide score of 2.
494 Tryptic peptides shared by multiple proteins were assigned to the winner
495 protein.

496

497 **RNA extraction and Array hybridization**

498 Total RNA was isolated from ATXN3^{shRNA} and SCR^{shRNA} cells using an
499 miRNeasy mini kit (Qiagen) and quality assessment was achieved using RNA
500 6000 Nano labchip (Bioanalyzer, Agilent) and by a Nanodrop
501 spectrophotometer (Thermo). Total RNAs RIN values were between 8.7 and
502 9.3 (average: 9.17). Affymetrix Human Transcriptome Array 2.0 ST arrays
503 were hybridized according Affymetrix recommendations using the Ambion WT

504 protocol (Life technologies, France) and Affymetrix labelling and hybridization
505 kits. Raw data, transcript data and exon data were controlled with Expression
506 console (Affymetrix).
507
508 **Microarray data analysis**
509 Affymetrix Human Transcriptome Array 2.0 ST dataset analysis was
510 performed using the GenoSplice technology (www.genosplice.com). Data was
511 normalized using quantile normalization. Background corrections were made
512 with antigenomic probes and probes were selected according to their %GC,
513 cross-hybridization status and potential overlap with repeat region as
514 previously described [PMID:23861464, PMID:23321315, PMID:23284676].
515 Only probes targeting exons and exon-exon junctions annotated from FAST
516 DB® transcripts (release fastdb_2013_2) were selected [PMID:16052034,
517 PMID:17547750]. Only probes with a DABG P value ≤0.05 in at least half of
518 the arrays were considered for statistical analysis [PMID:23861464,
519 PMID:23321315, PMID:23284676]. Only genes expressed in at least one
520 compared condition were analyzed. To be considered to be expressed, the
521 DABG P-value had to be ≤0.05 for at least half of the gene probes. We
522 performed an unpaired Student's *t-test* to compare gene intensities between
523 ATXN3^{shRNA} and SCR^{shRNA} cells. Genes were considered significantly
524 regulated when fold-change was ≥1.5 and P-value ≤0.05 (unadjusted P-
525 value). Analysis at the splicing level was first performed taking into account
526 only exon probes ('EXON analysis) in order to potentially detect new
527 alternative events that could be differentially regulated (i.e., without taking into
528 account exon-exon junction probes). Analysis at the splicing level was also

529 performed by taking into account exon-exon junction probes ('SPLICING
530 PATTERN analysis) using the FAST DB® splicing pattern annotation (i.e., for
531 each gene, all possible splicing patterns were defined and analyzed. All types
532 of alternative events can be analyzed: alternative first exons, alternative
533 terminal exons, cassette exon, mutually exclusive exons, alternative 5' donor
534 splice site, alternative 3' acceptor splice sites and intron retention). EXON and
535 SPLICING PATTERN analyses were performed using unpaired Student's *t-*
536 *test* on the splicing-index as previously described [PMID:23861464,
537 PMID:23321315, PMID:23284676]. Results were considered statistically
538 significant for unadjusted P-values ≤ 0.05 and fold-changes ≥ 1.5 for
539 SPLICING PATTERN analysis and unadjusted P-values ≤ 0.05 and fold-
540 changes ≥ 2.0 for EXON analysis. Gene Ontology (GO), KEGG and
541 REACTOME analyses of differentially regulated genes were performed using
542 DAVID [PMID:19131956].
543
544 **Plasmid purification**
545 Hybrid minigene reporter plasmids pyPY, AdML and α-globulin [31,32] were
546 kindly provided by Prof. Juan Valcárcel (Centre de Regulació Genòmica –
547 CRG, Barcelona). Top10 competent cells (Invitrogen) were transformed with
548 100 ng of plasmid DNA, according to the recommended protocol. Briefly, the
549 cells were incubated with the constructs on ice for 30 min followed by heat
550 shock at 42ºC for 1 min. After incubation on ice for 2 min, 500 µL of LB
551 medium was added to the cell vial and incubated at 150 rpm for 60 min at
552 37ºC. Cultures were grown overnight at 37ºC in LB/ampicillin plates. The next
553 day, one colony was inoculated in LB/ampicilin (100 mg/mL) at 37ºC

554 overnight. Plasmid extraction was carried out using the ZR Plasmid
555 Miniprep™ (Zymo Research) according with the manufacturer's protocol. DNA
556 concentration was determined using Nanodrop (Alfagene) and integrity
557 verified by running 200 ng in an agarose gel.
558
559 **Cell transfection**
560 $4x10^5$ cells per well were plated in gelatin-coated 6 well plates and incubated
561 for 24 h. Before transfection, the culture medium was changed to DMEM/F-
562 12-AA without antibiotics and supplemented with 5% FBS. Cells were
563 transfected with 200 ng of the reporter plasmids using Lipofectamine® 2000
564 Transfection Reagent (Invitrogen) according with the manufacturer's
565 instructions. Briefly, reporter plasmid minigenes and the transfection reagents
566 were appropriately diluted in Opti-MEM medium separately and incubated for
567 5 min at room temperature. The mixed reagents were then incubated at room
568 temperature for 20 min allowing the formation of transfection complexes. The
569 cells were then incubated for 24 h with the transfection mix.
570
571 **Semi-quantitative PCR**
572 PCR amplification of pyPY, AdML and α-globin reporter genes was carried out
573 using Taq DNA Polymerase (Thermo Fisher Scientific) following the
574 manufacturer's protocol. The cycling conditions were: 95ºC for 5 min followed
575 by 24 cycles of denaturing at 95ºC for 1 min, annealing at 60ºC for 45 sec,
576 extension at 72ºC for 1 min and final extension at 72ºC for 5 minutes. The
577 primers used are listed in Table S1. The PCR product was ran in a 2%

578 agarose gel. Gel analyses and splicing efficiency calculations were performed
579 using Image Lab software (Bio-Rad).
580
581 **Cell fractionation**
582 RA-treated pelleted cells were resuspended in ice RSB buffer (10 mM Tris-
583 HCl pH 7.4, 10 M NaCl) and incubated on ice 3 min. After centrifugation for 5
584 min, 4000 rpm at 4ºC, the pellet was resuspended in RSBG40 buffer (10 mM
585 Tris-HCl pH 7.4, 10 mM NaCl, 3 mM $MgCl_2$, 10% glycerol, 0.5% NP-40, 0,5
586 mM DTT) and centrifuged for 3 min, 7000 rpm at 4ºC. The supernatant was
587 collected as cytoplasmic fraction and stored at -80ºC. The nuclear pellet was
588 resuspended in 50 µL B1 buffer (20 mM Tris-HCl pH 7.9, 75 mM NaCl, 5%
589 glycerol, 0.5 mM EDTA, 0.85 mM DTT, 0.125 mM PMSF) and 450 µL B2
590 buffer (20 mM HEPES pH 7.6, 300 mM NaCl, 0.2 mM EDTA, 1 mM DTT, 7.5
591 mM $MgCl_2$, 1 M Urea, 1% NP-40). Samples were vortexed for 5 sec,
592 incubated on ice for 10 min and centrifuged for 5 min, 15000 rpm at 4ºC. The
593 supernatant was collected as nuclear fraction and stored at -80ºC.
594
595 **Protein synthesis inhibition and proteasome inhibition**
596 RA-treated SH-SY5Y cells were incubated with 5 µM cicloheximide (Merck)
597 during 20, 60 and 120 minutes. For proteasome inhibition, RA-treated cells
598 were incubated with 5 µM MG132 (Calbiochem) for 24h prior to lysis.
599
600 **High-throughput high-content functional imaging**
601 SH-SY5Y cells were seeded at a density of $4x10^3$ cells/well in flat bottom 96-
602 well plates previously coated with Matrigel (BD, Biosciences), and 10 µM all-

603 trans-retinoic acid (Sigma Aldrich) was added the day after plating in DMEM-
604 F12 with 1% FBS, to induce differentiation. After 5 days, cells were washed in
605 DMEM/F-12 and incubated with 50 ng/mL BDNF (Prepotech) in DMEM/F-12
606 without serum for 3 days. Cells were then labeled for β-III tubulin (1:1000,
607 R&D Systems), scanned at different locations of each well and the
608 quantitative analysis of neurite length were automatically done using the
609 automatic imaging system Thermo Scientific Cellomics® ArrayScan® VTI.
610
611 **Immunoprecipitation**
612 RA-treated cells were washed in ice-cold PBS and lysed by sonication on ice
613 in NP-40 buffer. Aliquots were taken from protein extracts as 10% inputs. 1
614 mg of total protein was pre-cleared for 3 h at 4ºC by incubation with
615 glutathione-coupled sepharose beads (GE Healthcare) previously equilibrated
616 in Wash buffer 1 (50 mM Tris-HCl pH 7.5, 150 nM NaCl, 1% NP-40, 1x
617 protease inhibitors (Roche)) for 3 times, 10 min at 4ºC. Beads were then
618 centrifuged and the supernatant was incubated O/N at 4ºC with 50 µL
619 equilibrated beads. After centrifugation, the supernatant was discarded and
620 the beads were washed 2 times with Wash buffer 1 for 10 min at 4ºC. Beads
621 were then washed twice with Wash buffer 2 (50 mM Tris-HCl pH 7.5, 500 mM
622 NaCl, 0.1% NP-40) for 10 min at 4ºC, and once with Wash buffer 3 (50 mM
623 Tris-HCL pH 7.5, 0.1% NP-40) for 20 min at 4ºC. The supernatant was
624 discarded and the bound proteins were eluted with 1x Laemmli buffer, boiled
625 for 5 min at 98ºC and run in a 10% SDS-PAGE gel.
626
627 **Proximity Ligation Assay (PLA)**

628 SH-SY5Y cells were cultured onto polyD-lysine coated cover slips in 24-well
629 plates using D-MEM media as indicated to above. PLA protocol was
630 performed as described in [67] and following manufacturer instructions with
631 adaptations. Cells were fixed with 4% PFA, and permeabilized with 0.5%
632 Triton in PBS at room temperature. Blocking was performed at 37ºC in a
633 humidity chamber for 1 hour, using Duolink® PLA Blocking Solution (Sigma).
634 Primary antibodies were incubated over night at 4ºC followed by two washing
635 steps of 5 minutes with Wash Buffer A (Sigma) at room temperature. PLUS
636 and MINUS PLA probes were diluted 1:5 in the Duolink Antibody Diluent
637 (Sigma), added to the cover slips and incubated for 1h at 37ºC in a humidity
638 chamber. Washing was performed for 5 minutes two times with Washing
639 Buffer A at room temperature followed by incubation with Ligase solution
640 (Sigma) for 30 minutes at 37ºC in a humidity chamber. After washing two
641 times during 2 minutes with Washing Buffer A at room temperature, cover
642 slips were incubated with Amplification solution (Sigma) for 100 minutes at
643 37ºC in a humidity chamber protected from light. Then, cover slips were
644 washed two times during 10 minutes with Washing Buffer B (Sigma) at room
645 temperature followed by an additional washing step of 1 minute using 100X
646 diluted Washing Buffer B. Cover slips were mounted on a glass slide with
647 mounting media and DAPI and cells analyzed by confocal microscopy.
648
649 **Immunoblotting**
650 RA-treated cells were pelleted and frozen in liquid nitrogen. For cellular and
651 brain tissue extracts, 50 µg of total protein isolated in NP-40 buffer (150 mM
652 NaCl, 50 mM Tris-HCl pH 7.6, 0.5% NP-40, protease inhibitors (Roche)) were

653 resolved in 10% SDS-PAGE gels and then transferred to a nitrocellulose
654 membrane. After incubation with the primary antibodies: Tau-5 (1:2000,
655 Abcam), Tau-4R (1:1000, Millipore), Tau-3R (1:2000, Millipore), Tau (E178)
656 (1:1000, Abcam), Histone H3 (1:10.000, Abcam), SFRS7(9G8) (1:1000, kindly
657 provided by Dr. James Stévine), Actin (1:200, DSHB) overnight at 4ºC,
658 membranes were incubated with secondary antibodies for 1 hour at room
659 temperature (anti-rabbit or anti-mouse, 1:10.000, Bio-Rad, anti-goat, 1:7500,
660 Pierce. Antibody binding was detected by chemiluminescence (Clarity kit, Bio-
661 Rad).
662
663 **qRT-PCR**
664 1 µg of total RNA purified from differentiated cells or brain tissue samples was
665 reversed transcribed using the One-step SuperScript kit (Bio-Rad). The qRT-
666 PCR reaction was performed in a CFX96 Real-time PCR detection system
667 (Bio-Rad) using the Quantitec SYBR Green kit (Qiagen) and the primers listed
668 on Table S1. Gene expression was normalized to *HMBS* or *B2M* levels within
669 each sample. Results are presented as fold change.
670
671 **Neurostructural analysis**
672 Mice were transcardially perfused with 0.9 % saline (n=9 per group) under
673 deep anesthesia (mixture of ketamine hydrochloride (150 mg/kg) plus
674 medetomidine (0.3 mg/kg)). Briefly, brains were immersed in Golgi-Cox
675 solution[68] for 14 days, processed and cut on a vibratome at 200 µm thick
676 coronal sections. For each selected neuron, all branches of the dendritic tree
677 were reconstructed at x1000 magnification, using a motorized microscope

(Zeiss, Thornwood) attached to a camera (Sony) and Neurolucida software (Microbrightfield). A three-dimensional analysis of the reconstructed neurons was performed using NeuroExplorer software (Microbrightfield).

Quantification and statistical analysis

Continuous variables with normal distributions (Shapiro-Wilk test $p>0.05$) were analyzed with the Student *t-test* or two-way ANOVA. Non-parametric Mann-Whitney U-test was used when variables were non-continuous or when a continuous variable did not present a normal distribution (Shapiro-Wilk test $p<0.05$). All statistical analysis were performed using SPSS 22.0 (SPSS Inc., Chicago, IL). A critical value for significance of $p<0.05$ was used throughout the study. For real-time quantitative PCR data, the same approach was used and results were presented using the ΔΔCt method, as described before [69].

AUTHOR CONTRIBUTIONS

Conceptualization, ANC and PM; Methodology, ANC, PM, IS, SH, PH and KWL; Formal analysis, ANC and KWL; Investigation, ANC, BA, SDS, JS, SH and KWL; Writing – original draft, ANC; Writing – review & editing, ANC, PM, IS, PH and KWL; Visualization, ANC; Funding acquisition, PM; Resources, PM, KWL, PH; Supervision, PM

ACKNOWLEDGMENTS

This article has been developed under the scope of the project NORTE-01-0145-FEDER-000013, supported by the Northern Portugal Regional Operational Programme (NORTE 2020), under the Portugal 2020 Partnership

Agreement, through the European Regional Development Fund (FEDER). This work has been funded by FEDER funds, through the Competitiveness Factors Operational Programme (COMPETE), and by National funds, through the Foundation for Science and Technology (FCT), under the scope of the project POCI-01-0145-FEDER-007038 and through the project POCI-01-0145-FEDER-016818 (PTDC/NEU-NMC/3648/2014) and fellowships [SFRH/BD/51059/2019 to A. N-C, SFRH/BPD/110728/2015 to B.A, SFRH/BD/78388/2011 to S.D-S, SFRH/BD/88932/2012 to J.M.S and IF/01799/2013 to I.S.

CONFLIT OF INTEREST

The authors declare no conflict of interest.

REFERENCES

1. Hegde, A.N. & Upadhya, S.C. Role of ubiquitin-proteasome-mediated proteolysis in nervous system disease. *Biochim Biophys Acta* **1809**, 128-140 (2011).
2. Yi, J.J. & Ehlers, M.D. Emerging roles for ubiquitin and protein degradation in neuronal function. *Pharmacol Rev* **59**, 14-39 (2007).
3. Baptista, M.S., Duarte, C.B. & Maciel, P. Role of the ubiquitin-proteasome system in nervous system function and disease: using C. elegans as a dissecting tool. *Cell Mol Life Sci* **69**, 2691-2715 (2012).
4. Hershko, A. & Ciechanover, A. The ubiquitin system. *Annu Rev Biochem* **67**, 425-479 (1998).

728 5. Komander, D. The emerging complexity of protein ubiquitination.
729 *Biochem Soc Trans* **37**, 937-953 (2009).
730 6. Tai, H.C. & Schuman, E.M. Ubiquitin, the proteasome and protein
731 degradation in neuronal function and dysfunction. *Nat Rev Neurosci* **9**,
732 826-838 (2008).
733 7. de Vrij, F.M., Fischer, D.F., van Leeuwen, F.W. & Hol, E.M. Protein quality
734 control in Alzheimer's disease by the ubiquitin proteasome system. *Prog*
735 *Neurobiol* **74**, 249-270 (2004).
736 8. Upadhya, S.C. & Hegde, A.N. Ubiquitin-proteasome pathway components
737 as therapeutic targets for CNS maladies. *Curr Pharm Des* **11**, 3807-3828
738 (2005).
739 9. Rubinsztein, D.C. The roles of intracellular protein-degradation pathways
740 in neurodegeneration. *Nature* **443**, 780-786 (2006).
741 10. Nijman, S.M.*, et al.* A genomic and functional inventory of deubiquitinating
742 enzymes. *Cell* **123**, 773-786 (2005).
743 11. Komander, D., Clague, M.J. & Urbe, S. Breaking the chains: structure and
744 function of the deubiquitinases. *Nat Rev Mol Cell Biol* **10**, 550-563 (2009).
745 12. Clague, M.J., Coulson, J.M. & Urbe, S. Cellular functions of the DUBs. *J Cell*
746 *Sci* **125**, 277-286 (2012).
747 13. Rappsilber, J., Ryder, U., Lamond, A.I. & Mann, M. Large-scale proteomic
748 analysis of the human spliceosome. *Genome Res* **12**, 1231-1245 (2002).
749 14. Makarov, E.M.*, et al.* Small nuclear ribonucleoprotein remodeling during
750 catalytic activation of the spliceosome. *Science* **298**, 2205-2208 (2002).

751 15. Wagner, S.A., *et al.* A proteome-wide, quantitative survey of in vivo
752 ubiquitylation sites reveals widespread regulatory roles. *Mol Cell*
753 *Proteomics* **10**, M111 013284 (2011).
754 16. Peng, J., *et al.* A proteomics approach to understanding protein
755 ubiquitination. *Nat Biotechnol* **21**, 921-926 (2003).
756 17. Bellare, P., Kutach, A.K., Rines, A.K., Guthrie, C. & Sontheimer, E.J. Ubiquitin
757 binding by a variant Jab1/MPN domain in the essential pre-mRNA
758 splicing factor Prp8p. *RNA* **12**, 292-302 (2006).
759 18. Kramer, A., Mulhauser, F., Wersig, C., Groning, K. & Bilbe, G. Mammalian
760 splicing factor SF3a120 represents a new member of the SURP family of
761 proteins and is homologous to the essential splicing factor PRP21p of
762 Saccharomyces cerevisiae. *RNA* **1**, 260-272 (1995).
763 19. Lygerou, Z., Christophides, G. & Seraphin, B. A novel genetic screen for
764 snRNP assembly factors in yeast identifies a conserved protein, Sad1p,
765 also required for pre-mRNA splicing. *Mol Cell Biol* **19**, 2008-2020 (1999).
766 20. Makarova, O.V., Makarov, E.M. & Luhrmann, R. The 65 and 110 kDa SR-
767 related proteins of the U4/U6.U5 tri-snRNP are essential for the assembly
768 of mature spliceosomes. *EMBO J* **20**, 2553-2563 (2001).
769 21. Burnett, B., Li, F. & Pittman, R.N. The polyglutamine neurodegenerative
770 protein ataxin-3 binds polyubiquitylated proteins and has ubiquitin
771 protease activity. *Hum Mol Genet* **12**, 3195-3205 (2003).
772 22. Doss-Pepe, E.W., Stenroos, E.S., Johnson, W.G. & Madura, K. Ataxin-3
773 interactions with rad23 and valosin-containing protein and its
774 associations with ubiquitin chains and the proteasome are consistent

775 with a role in ubiquitin-mediated proteolysis. *Mol Cell Biol* **23**, 6469-6483
776 (2003).
777 23. Rodrigues, A.J., *et al.* Absence of ataxin-3 leads to cytoskeletal
778 disorganization and increased cell death. *Biochim Biophys Acta* **1803**,
779 1154-1163 (2010).
780 24. do Carmo Costa, M., *et al.* Ataxin-3 plays a role in mouse myogenic
781 differentiation through regulation of integrin subunit levels. *PLoS One* **5**,
782 e11728 (2010).
783 25. Neves-Carvalho, A., *et al.* Dominant negative effect of polyglutamine
784 expansion perturbs normal function of ataxin-3 in neuronal cells. *Hum*
785 *Mol Genet* **24**, 100-117 (2015).
786 26. Zhong, X. & Pittman, R.N. Ataxin-3 binds VCP/p97 and regulates
787 retrotranslocation of ERAD substrates. *Hum Mol Genet* **15**, 2409-2420
788 (2006).
789 27. Wang, G., Sawai, N., Kotliarova, S., Kanazawa, I. & Nukina, N. Ataxin-3, the
790 MJD1 gene product, interacts with the two human homologs of yeast DNA
791 repair protein RAD23, HHR23A and HHR23B. *Hum Mol Genet* **9**, 1795-
792 1803 (2000).
793 28. Chatterjee, A., *et al.* The role of the mammalian DNA end-processing
794 enzyme polynucleotide kinase 3'-phosphatase in spinocerebellar ataxia
795 type 3 pathogenesis. *PLoS Genet* **11**, e1004749 (2015).
796 29. Gao, R., *et al.* Inactivation of PNKP by mutant ATXN3 triggers apoptosis by
797 activating the DNA damage-response pathway in SCA3. *PLoS Genet* **11**,
798 e1004834 (2015).

799 30. Hjerpe, R., *et al.* Efficient protection and isolation of ubiquitylated
800 proteins using tandem ubiquitin-binding entities. *EMBO Rep* **10**, 1250-
801 1258 (2009).
802 31. Guth, S., Martinez, C., Gaur, R.K. & Valcarcel, J. Evidence for substrate-
803 specific requirement of the splicing factor U2AF(35) and for its function
804 after polypyrimidine tract recognition by U2AF(65). *Mol Cell Biol* **19**,
805 8263-8271 (1999).
806 32. Pacheco, T.R., Coelho, M.B., Desterro, J.M., Mollet, I. & Carmo-Fonseca, M.
807 In vivo requirement of the small subunit of U2AF for recognition of a
808 weak 3' splice site. *Mol Cell Biol* **26**, 8183-8190 (2006).
809 33. Cavaloc, Y., Popielarz, M., Fuchs, J.P., Gattoni, R. & Stevenin, J.
810 Characterization and cloning of the human splicing factor 9G8: a novel 35
811 kDa factor of the serine/arginine protein family. *EMBO J* **13**, 2639-2649
812 (1994).
813 34. Silva-Fernandes, A., *et al.* Chronic treatment with 17-DMAG improves
814 balance and coordination in a new mouse model of Machado-Joseph
815 disease. *Neurotherapeutics* **11**, 433-449 (2014).
816 35. Lopitz-Otsoa, F., *et al.* Integrative analysis of the ubiquitin proteome
817 isolated using Tandem Ubiquitin Binding Entities (TUBEs). *J Proteomics*
818 **75**, 2998-3014 (2012).
819 36. Li, K.W., *et al.* Identifying true protein complex constituents in interaction
820 proteomics: the example of the DMXL2 protein complex. *Proteomics* **12**,
821 2428-2432 (2012).
822 37. Ule, J. & Darnell, R.B. RNA binding proteins and the regulation of neuronal
823 synaptic plasticity. *Curr Opin Neurobiol* **16**, 102-110 (2006).

824 38. Anderson, P. & Ivanov, P. tRNA fragments in human health and disease.
825 *FEBS Lett* **588**, 4297-4304 (2014).
826 39. Belzil, V.V., Gendron, T.F. & Petrucelli, L. RNA-mediated toxicity in
827 neurodegenerative disease. *Mol Cell Neurosci* **56**, 406-419 (2013).
828 40. Bentmann, E., Haass, C. & Dormann, D. Stress granules in
829 neurodegeneration--lessons learnt from TAR DNA binding protein of 43
830 kDa and fused in sarcoma. *FEBS J* **280**, 4348-4370 (2013).
831 41. Ling, S.C., Polymenidou, M. & Cleveland, D.W. Converging mechanisms in
832 ALS and FTD: disrupted RNA and protein homeostasis. *Neuron* **79**, 416-
833 438 (2013).
834 42. Halliday, G.*, et al.* Mechanisms of disease in frontotemporal lobar
835 degeneration: gain of function versus loss of function effects. *Acta*
836 *Neuropathol* **124**, 373-382 (2012).
837 43. Busch, A. & Hertel, K.J. Evolution of SR protein and hnRNP splicing
838 regulatory factors. *Wiley Interdiscip Rev RNA* **3**, 1-12 (2012).
839 44. Moulton, V.R., Gillooly, A.R. & Tsokos, G.C. Ubiquitination regulates
840 expression of the serine/arginine-rich splicing factor 1 (SRSF1) in normal
841 and systemic lupus erythematosus (SLE) T cells. *J Biol Chem* **289**, 4126-
842 4134 (2014).
843 45. Breig, O. & Baklouti, F. Proteasome-mediated proteolysis of SRSF5
844 splicing factor intriguingly co-occurs with SRSF5 mRNA upregulation
845 during late erythroid differentiation. *PLoS One* **8**, e59137 (2013).
846 46. Graveley, B.R. Sorting out the complexity of SR protein functions. *RNA* **6**,
847 1197-1211 (2000).

848 47. Fu, X.D. The superfamily of arginine/serine-rich splicing factors. *RNA* **1**,
849 663-680 (1995).
850 48. Gao, L., Wang, J., Wang, Y. & Andreadis, A. SR protein 9G8 modulates
851 splicing of tau exon 10 via its proximal downstream intron, a clustering
852 region for frontotemporal dementia mutations. *Mol Cell Neurosci* **34**, 48-
853 58 (2007).
854 49. Ding, S.*, et al.* Regulation of alternative splicing of tau exon 10 by 9G8 and
855 Dyrk1A. *Neurobiol Aging* **33**, 1389-1399 (2012).
856 50. Goedert, M., Spillantini, M.G., Jakes, R., Rutherford, D. & Crowther, R.A.
857 Multiple isoforms of human microtubule-associated protein tau:
858 sequences and localization in neurofibrillary tangles of Alzheimer's
859 disease. *Neuron* **3**, 519-526 (1989).
860 51. Goedert, M. & Jakes, R. Expression of separate isoforms of human tau
861 protein: correlation with the tau pattern in brain and effects on tubulin
862 polymerization. *EMBO J* **9**, 4225-4230 (1990).
863 52. Yin, X.*, et al.* Dyrk1A overexpression leads to increase of 3R-tau
864 expression and cognitive deficits in Ts65Dn Down syndrome mice. *Sci Rep*
865 **7**, 619 (2017).
866 53. Magdalinou, N.K.*, et al.* Identification of candidate cerebrospinal fluid
867 biomarkers in parkinsonism using quantitative proteomics. *Parkinsonism*
868 *Relat Disord* **37**, 65-71 (2017).
869 54. Luk, C.*, et al.* Development and assessment of sensitive immuno-PCR
870 assays for the quantification of cerebrospinal fluid three- and four-repeat
871 tau isoforms in tauopathies. *J Neurochem* **123**, 396-405 (2012).

872 55. Chen, S., Townsend, K., Goldberg, T.E., Davies, P. & Conejero-Goldberg, C.
873 MAPT isoforms: differential transcriptional profiles related to 3R and 4R
874 splice variants. *J Alzheimers Dis* **22**, 1313-1329 (2010).
875 56. Sennvik, K., *et al.* Tau-4R suppresses proliferation and promotes neuronal
876 differentiation in the hippocampus of tau knockin/knockout mice. *FASEB*
877 *J* **21**, 2149-2161 (2007).
878 57. Winborn, B.J., *et al.* The deubiquitinating enzyme ataxin-3, a
879 polyglutamine disease protein, edits Lys63 linkages in mixed linkage
880 ubiquitin chains. *J Biol Chem* **283**, 26436-26443 (2008).
881 58. Singh, N.N. & Singh, R.N. Alternative splicing in spinal muscular atrophy
882 underscores the role of an intron definition model. *RNA Biol* **8**, 600-606
883 (2011).
884 59. Orozco, D. & Edbauer, D. FUS-mediated alternative splicing in the nervous
885 system: consequences for ALS and FTLD. *J Mol Med (Berl)* **91**, 1343-1354
886 (2013).
887 60. Mills, J.D. & Janitz, M. Alternative splicing of mRNA in the molecular
888 pathology of neurodegenerative diseases. *Neurobiol Aging* **33**, 1012
889 e1011-1024 (2012).
890 61. Ranum, L.P. & Cooper, T.A. RNA-mediated neuromuscular disorders. *Annu*
891 *Rev Neurosci* **29**, 259-277 (2006).
892 62. Sun, J., Xu, H., Negi, S., Subramony, S.H. & Hebert, M.D. Differential effects
893 of polyglutamine proteins on nuclear organization and artificial reporter
894 splicing. *J Neurosci Res* **85**, 2306-2317 (2007).
895 63. Silva-Fernandes, A., *et al.* Motor uncoordination and neuropathology in a
896 transgenic mouse model of Machado-Joseph disease lacking intranuclear

897 inclusions and ataxin-3 cleavage products. *Neurobiol Dis* **40**, 163-176
898 (2010).
899 64. Nicklas, W.*, et al.* Recommendations for the health monitoring of rodent
900 and rabbit colonies in breeding and experimental units. *Lab Anim* **36**, 20-
901 42 (2002).
902 65. Colledge, M.*, et al.* Targeting of PKA to glutamate receptors through a
903 MAGUK-AKAP complex. *Neuron* **27**, 107-119 (2000).
904 66. Shilov, I.V.*, et al.* The Paragon Algorithm, a next generation search engine
905 that uses sequence temperature values and feature probabilities to
906 identify peptides from tandem mass spectra. *Mol Cell Proteomics* **6**, 1638-
907 1655 (2007).
908 67. Fredriksson, S.*, et al.* Protein detection using proximity-dependent DNA
909 ligation assays. *Nat Biotechnol* **20**, 473-477 (2002).
910 68. Glaser, E.M. & Van der Loos, H. Analysis of thick brain sections by
911 obverse-reverse computer microscopy: application of a new, high clarity
912 Golgi-Nissl stain. *J Neurosci Methods* **4**, 117-125 (1981).
913 69. Pfaffl, M.W. A new mathematical model for relative quantification in real-
914 time RT-PCR. *Nucleic Acids Res* **29**, e45 (2001).
915

916 **FIGURE LEGENDS**

917 **Figure 1.** Experimental design – purification of polyubiquitylated proteins
918 using TUBEs. **(A-I)** RA-treated SH-SY5Y cells (with silenced ATXN3 or not)
919 were lysed and protein extracts were incubated with TUBEs. **(A-II)** TUBEs-
920 captured proteins were recovered with Laemmli buffer and analyzed by

921 comassie blue staining of the polyubiquityated proteins purified using TUBEs
922 run in a 1-D SDS-PAGE gel or western-blot with anti-ubiquitin FK2 antibody.
923 **(A-III)** Polyubiquitylated proteins were trypsin-digested and identified by LC-
924 MS/MS. **(B)** After acquisition, data were processed and integrated in
925 functional networks.
926
927 **Table 1.** RNA metabolism related proteins with altered ubiquitylation in cells
928 lacking ATXN3.
929
930 **Figure 2.** Efficacy of RNA processing assessed by splicing reporter
931 minigenes in ATXN3^{shRNA} cells. **(A-E)** Semi-quantitative analysis of minigene'
932 alternative splicing showed a decreased efficiency of splicing in **(A-D)**
933 ATXN3^{shRNA} cells and **(E)** ATXN3_C14A cells. Schemes for the splicing
934 products are indicated on the left right. Exons are represented as colored
935 boxes and introns by red lines. The AdML minigene contains one intron,
936 giving rise to two bands: the upper band corresponds to the unspliced
937 transcript, the lower band to the spliced product. The pyPY minigene contains
938 two alternative splice sites originating three bands: an upper band
939 corresponding to the unspliced transcript, a middle band corresponding to the
940 splicing of the weak py tract and a lower band corresponding to the splicing
941 product of the strong PY tract. The pyPY minigene contains two alternative 3'
942 splice sites associated with polypirimidine (Py) tracts with different strengths.
943 The weak Py tract (py) is represented by thin red lines and the strong Py tract
944 (PY) by a thick red line. The α-globin minigene contains two introns and a set
945 of G triplets in intron 2 that promote the recognition of the 5' splice site leading

946 to skipping of exon 2. **(F)** Experimental design – microarray analysis of
947 alternative splicing using the Affymetrix Human Transcriptome Array 2.0 ST to
948 assess perturbation of global splicing patterns in ATXN3^{shRNA} cells. **(G)**
949 Distribution of the differentially regulated alternative splicing events in
950 ATXN3^{shRNA} cells. n≥3 independent biological replicates in all experiments.
951 p<0,05 was taken as the cut-off. T-test was used for comparisons. Asterisks
952 represent mean ± standard deviation. *p<0,05; **p<0,01; ***p<0,001.
953
954 **Figure 3.** ATXN3^{shRNA} cells showed decreased SRSF7 protein levels. **(A-B)**
955 Western-blot analysis after capture of polyubiquitylated proteins confirmed the
956 decrease in polyubiquitylated forms of SRSF7 in ATXN3^{shRNA} cells. **(A-D)**
957 Downregulation of both **(A-B)** total and **(C-D)** nuclear SRSF7 protein levels in
958 ATXN3^{shRNA} cells. (**E-F)** Protein levels of SRSF7 are increased in ATXN3^{shRNA}
959 cells upon proteasome inhibition (MG132 treatment). **(G)** Western-blot
960 analysis after capture of polyubiquitylated proteins with K48-linked
961 polyubiquitin chains showed decrease levels in K48-polyubiquitylated forms of
962 SRSF7 in ATXN3^{shRNA} cells. Relative band density for each protein was
963 analyzed. The results were normalized for Histone H3. **(H)** Relative amounts
964 of SRSF7 in SCR^{shRNA} cells and ATXN3^{shRNA} cells at various cycloheximide
965 treatment times. Human ATXN3 co- interacts both **(I)** *in vitro* and **(J)** *in situ*
966 with SRSF7. Scale bar corresponds to 40 µm. n≥3 independent biological
967 replicates in all experiments. T-test or ANOVA were used for comparisons.
968 Asterisks represent mean ± standard deviation. *p<0.05; **p<0.01, ***p<0.01.
969

970 **Figure 4.** Disruption of 4R/3R-Tau ratio in ATXN3^{shRNA} cells. **(A)** qRT-PCR
971 analysis showed that silencing of ATXN3 lead to decreased transcription
972 levels of 4R-Tau, **(B)** no alterations in the mRNA levels of the 3R-Tau isoform,
973 **(C)** a significant decrease of the 4R/3R-Tau ratio and **(D)** decreased levels of
974 total Tau, both in ATXN3^{shRNA} cells and in **(E-H)** cerebellar primary neurons.
975 **(I)** ATXN3_C14A cells present decreased mRNA levels of 4R-Tau isoform, **(J)**
976 no alterations in 3R-Tau expression, **(K)** decreased 4R/3R-Tau ratio and **(L)**
977 decreased levels of total Tau. **(M)** SH-SY5Y ATXN3^{shRNA} cultures presented a
978 decreased expression of βIII-tubulin as assessed by immunostaining. **(N)** The
979 average length of the neuritis was reduced in ATXN3^{shRNA} cells as compared
980 with the SCR^{shRNA} controls. 4R/3R-Tau ratio was obtained by dividing 4R and
981 3R-Tau mRNA levels. n≥3 independent biological replicates in all
982 experiments. T-test was used for comparisons. Asterisks represent mean ±
983 standard deviation. ***p<0.001.
984
985 **Figure 5.** PolyQ expansion in ATXN3 affects Tau splicing. **(A)** Semi-
986 quantitative analysis of minigene' alternative splicing showed a decreased
987 efficiency of splicing in ATXN3_83Q cells. **(B)** Expression of ATXN3_83Q led
988 to decreased mRNA levels of 4R-Tau isoform, **(C)** no alterations in 3R-Tau
989 expression, **(D)** decreased 4R/3R-Tau ratio, and **(E)** decreased levels of total
990 Tau. **(F)** Tg mice presented a decrease in the mRNA levels of 4R-Tau, **(G)** no
991 alterations in expression of 3R-Tau, **(H)** a decreased 4R/3R-Tau ratio, and **(I)**
992 a decrease in the levels of total Tau comparing with Wt controls. **(J-L)** Tg
993 mice showed decreased Sfrs7 protein levels in different disease-affected
994 brain areas. **(M)** Decreased SRSF7 protein levels in SCA3 patient's brains.

995 **(N-P)** Decreased total dendritic length and dendritic tree complexity of
996 brainstem neurons in the Tg mice.
997 mRNA levels were normalized to the *HMBS* or *Hprt* genes. Relative band
998 density for each protein was analyzed. The results were normalized for actin
999 levels. n≥3 independent biological replicates in all experiments. T-test or
1000 ANOVA were used for comparisons. Asterisks represent mean ± standard
1001 deviation. *p<0.05; **p<0.01; ***p<0.001.
1002
1003 **Table S1.** Differences in polyubiquitylated proteins identified by TUBEs-MS in
1004 SH-SY5Y cells lacking ATXN3. List of identified proteins with altered levels of
1005 ubiquitylation in RA-treated ATXN3^{shRNA} cells as compared with the SCR^{shRNA}
1006 controls (p<0.05). These proteins were present in at least 3 independent
1007 experiments. The values are the average of "unused" values given by the
1008 Proteinpilot algorithm. The absent "unused" values indicate the (near)
1009 complete absence of the polyubiquitylated protein. In red and green are
1010 proteins with increased and decreased polyubiquitylated levels, respectively.
1011 $ indicates protein splicing factors.
1012
1013 **Figure EV1.** No changes in the mRNA levels of SRSF7 in ATXN3^{shRNA} cells
1014 and in the CMVMJD135 mice. **(A-B)** Percentage of ATXN3 silencing using
1015 different shRNA clones as compared to the scrambled sequence and empty
1016 vector expression. The different generated cell lines showed a similar
1017 phenotype. **(C)** No significant differences were observed in the mRNA levels
1018 of SRSF7 between the ATXN3^{shRNA} cells and the SCR^{shRNA} controls. **(D)**
1019 Knockdown of Atxn3 in cerebellar primary neurons. **(E)** PLA negative control

1020 (no antibodies) **(F)** No significant differences were observed in the mRNA
1021 levels of Srsf7 in the Tg mice as compared with the Wt-littermates controls.
1022 mRNA levels were normalized to the *HMBS* or *Hprt* genes. Relative band
1023 density for each protein was analyzed. The results were normalized for actin
1024 levels. n≥3 independent biological replicates in all experiments. T-test was
1025 used for comparisons. Asterisks represent mean ± standard deviation.
1026 *p<0.05.
1027
1028 **Table EV1.** Differentially regulated alternative splicing events in ATXN3^{shRNA}
1029 cells. List of genes with altered splicing in RA-treated ATXN3^{shRNA} cells as
1030 compared with the SCR^{shRNA} controls.
1031
1032 **Table EV2.** KEGG pathway analysis of genes with altered splicing in
1033 ATXN3^{shRNA} cells. The genes identified on the KEGG pathway analysis
1034 presented at least one differentially regulated exon/splicing pattern in
1035 ATXN3^{shRNA} cells.
1036
1037 **Table EV3.** Changes in alternative types events in ATXN3^{shRNA} cells.
1038

Figure 1

A

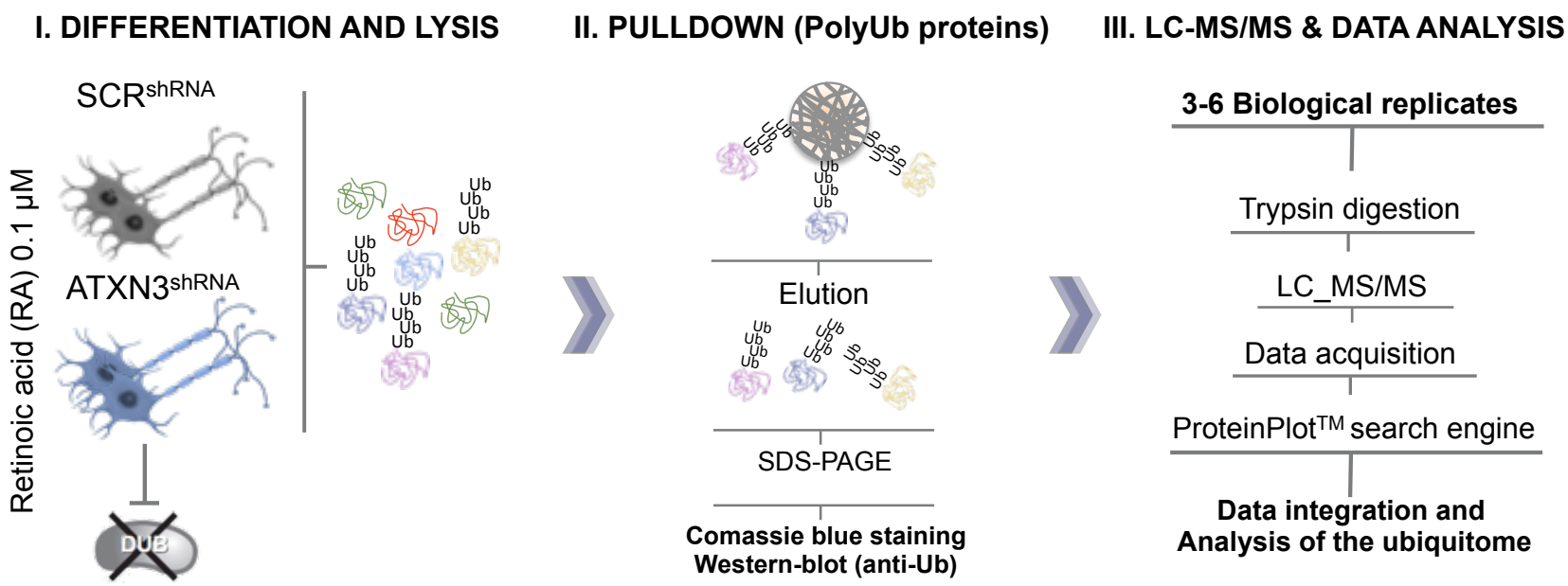
I. DIFFERENTIATION AND LYSIS
II. PULLDOWN (PolyUb proteins)
III. LC-MS/MS & DATA ANALYSIS
SCRshRNA
ATXN3shRNA
Retinoic acid (RA) 0.1 µM
DUB
Ub
Elution
SDS-PAGE
Comassie blue staining
Western-blot (anti-Ub)
3-6 Biological replicates
Trypsin digestion
LC_MS/MS
Data acquisition
ProteinPlot™ search engine
Data integration and
Analysis of the ubiquitome

B

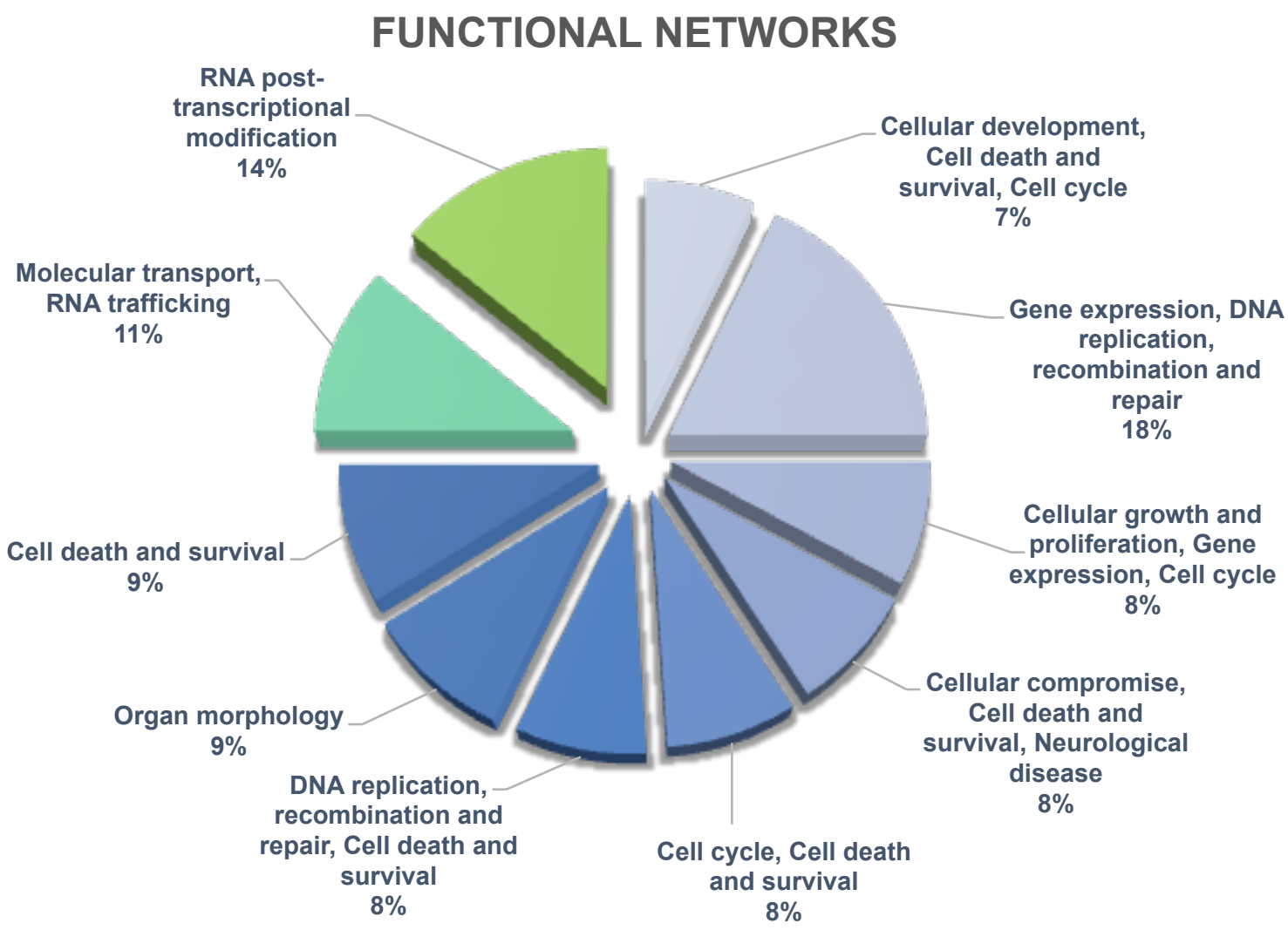
FUNCTIONAL NETWORKS
RNA post-transcriptional modification 14%
Cellular development, Cell death and survival, Cell cycle 7%
Molecular transport, RNA trafficking 11%
Gene expression, DNA replication, recombination and repair 18%
Cell death and survival 9%
Cellular growth and proliferation, Gene expression, Cell cycle 8%
Organ morphology 9%
Cellular compromise, Cell death and survival, Neurological disease 8%
DNA replication, recombination and repair, Cell death and survival 8%
Cell cycle, Cell death and survival 8%

Table 1

RNA METABOLISM PROTEINS WITH ALTERED UBIQUITYLATION IN ATXN3^{shRNA} CELLS

UPREGULATED	p value
RBM10 (RNA-binding protein 10)	4,87E-19
SNRPB2 (U2 small nuclear ribonucleoprotein B)	3,26E-11
SFRS2 (Splicing factor arginine/serine-rich 2)	5,36E-11
RBM8A (RNA-binding protein 8A)	1,56E-06
PRPF8 (Pre-mRNA-processing-splicing factor 8)	1,00E-03
SFRS5 (Serine/arginine-rich splicing factor 5)	5,00E-03
SNRPN (Small nuclear ribonucleoprotein-associated protein N)	5,00E-03
SRSF9 (Serine/arginine-rich splicing factor 9)	7,00E-03
RBM12B (RNA-binding protein 12B)	2,00E-02
AQR (Intron-binding protein aquarius)	2,00E-02
PRPF40A (Pre-mRNA-processing factor 40 homolog A)	2,00E-02
HNRNPK (Heterogeneous nuclear ribonucleoprotein K)	3,00E-02
DOWNREGULATED	**p value**
DDX41 (DEAD-box protein abstrakt variant)	6,22E-06
DDX56 (ATP-dependent RNA helicase)	2,38E-05
LUC7L (Putative RNA-binding protein Luc-like 1)	5,00E-04
SFRS7 (Serine/arginine-rich splicing factor)	8,00E-04
DDX10 (Probable ATP-dependent RNA helicase)	1,00E-02
HNRNPA1P10 (Heterogeneous nuclear ribonucleoprotein N)	2,00E-02
FUS (RNA-binding protein)	3,00E-02
RBMX (Heterogeneous nuclear ribonucleoprotein G)	4,00E-02
SRRT (Serrate RNA effector molecule)	4,00E-02

Figure 2

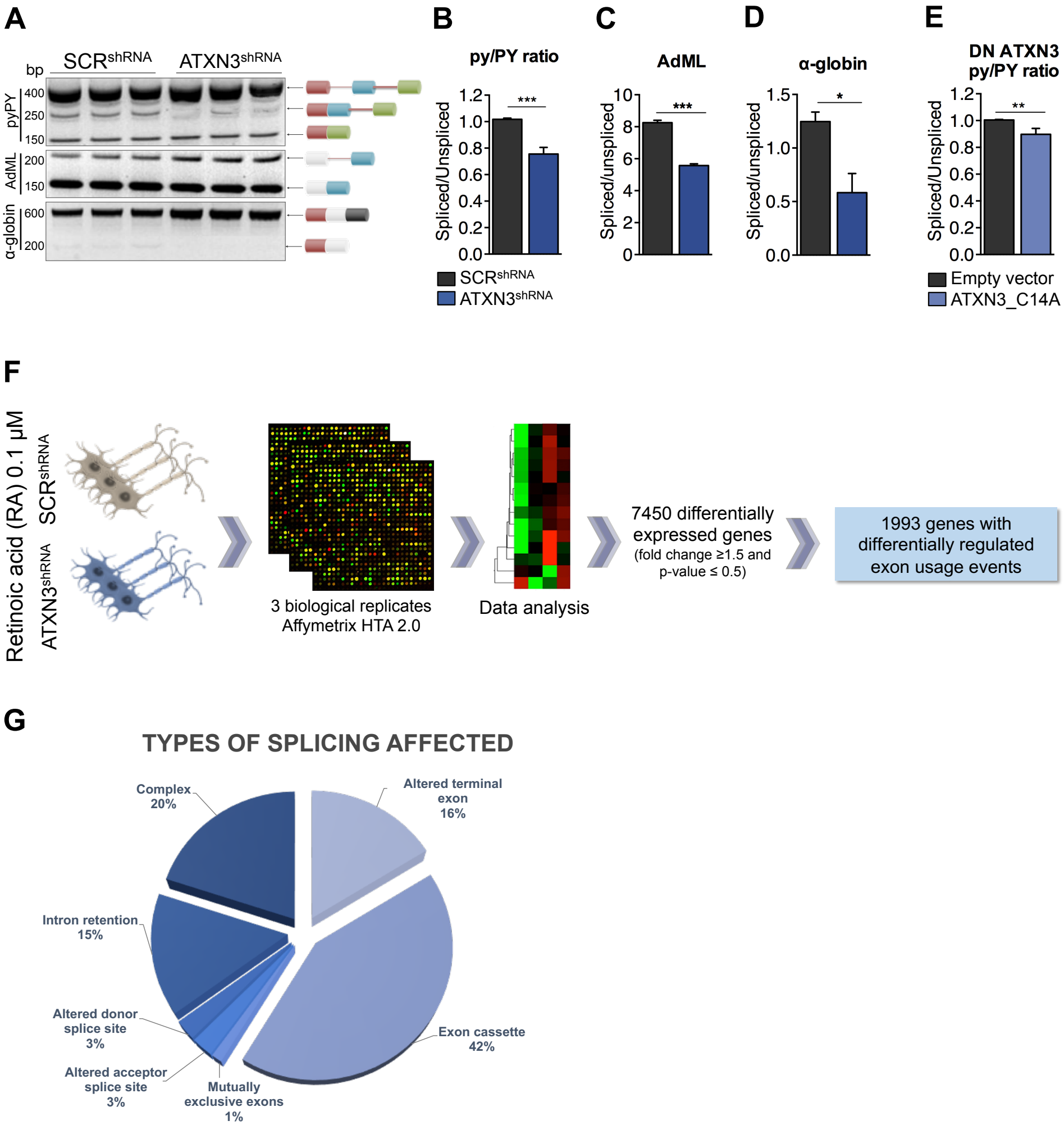
A
SCRshRNA
ATXN3shRNA
bp
pyPY
400
250
150
AdML
200
150
α-globin
600
200
B
py/PY ratio
Spliced/Unspliced
1.2
1.0
0.8
0.6
0.4
0.2
0.0
***
SCRshRNA
ATXN3shRNA
C
AdML
Spliced/unspliced
10
8
6
4
2
0
***
D
α-globin
Spliced/unspliced
1.5
1.0
0.5
0.0
*
E
DN ATXN3
py/PY ratio
Spliced/Unspliced
1.2
1.0
0.8
0.6
0.4
0.2
0.0
**
Empty vector
ATXN3_C14A
F
Retinoic acid (RA) 0.1 μM
SCRshRNA
ATXN3shRNA
3 biological replicates
Affymetrix HTA 2.0
Data analysis
7450 differentially
expressed genes
(fold change ≥1.5 and
p-value ≤ 0.5)
1993 genes with
differentially regulated
exon usage events
G
TYPES OF SPLICING AFFECTED
Complex
20%
Altered terminal
exon
16%
Intron retention
15%
Altered donor
splice site
3%
Altered acceptor
splice site
3%
Mutually
exclusive exons
1%
Exon cassette
42%

Figure 3

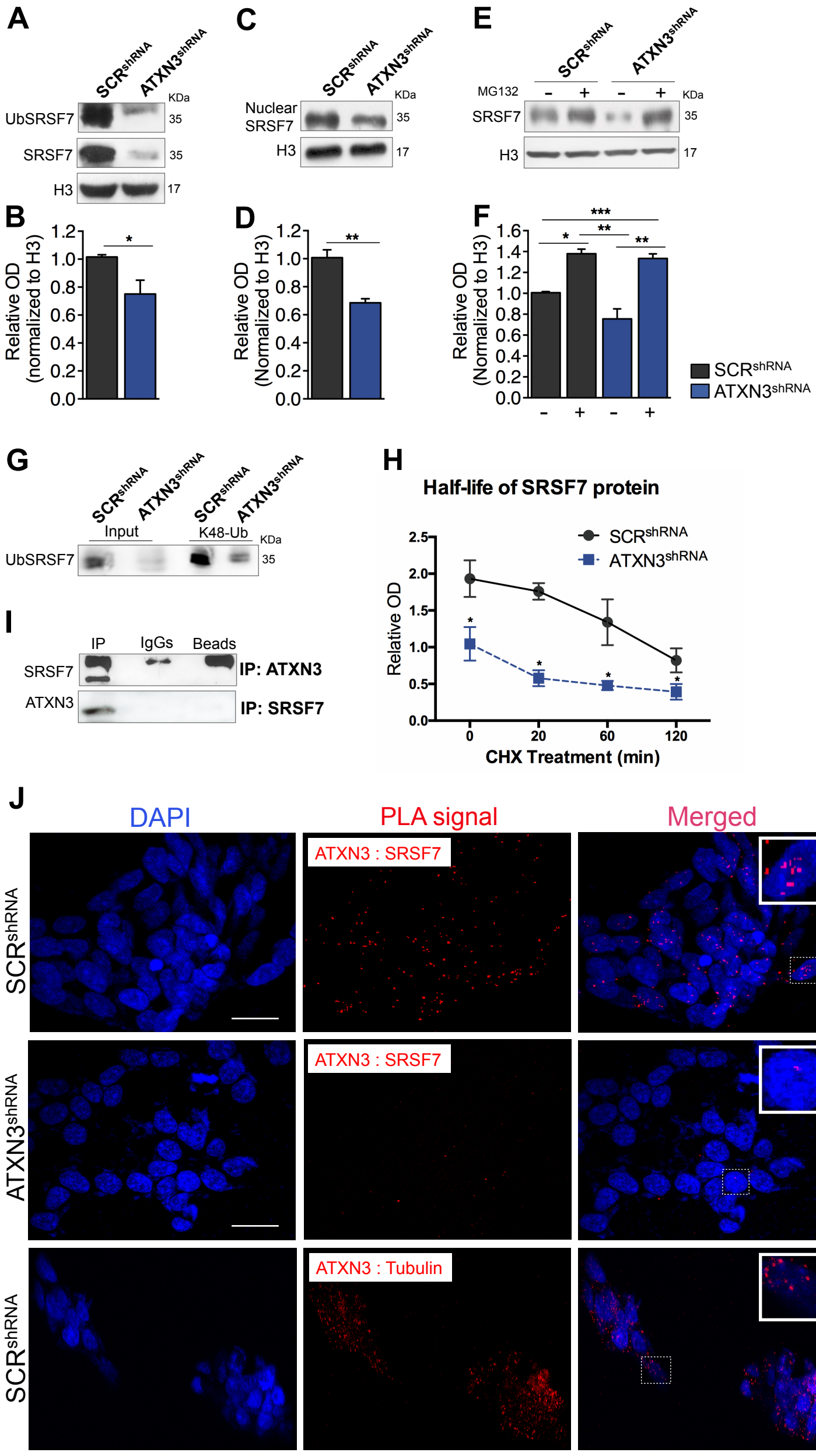
A
SCRshRNA
ATXN3shRNA
KDa
UbSRSF7
SRSF7
H3
35
35
17
B
Relative OD (normalized to H3)
C
Nuclear SRSF7
H3
D
Relative OD (Normalized to H3)
E
MG132
SRSF7
H3
F
Relative OD (Normalized to H3)
G
Input
K48-Ub
UbSRSF7
H
Half-life of SRSF7 protein
Relative OD
CHX Treatment (min)
I
IP
IgGs
Beads
SRSF7
ATXN3
IP: ATXN3
IP: SRSF7
J
DAPI
PLA signal
Merged
ATXN3 : SRSF7
ATXN3 : Tubulin

Figure 4

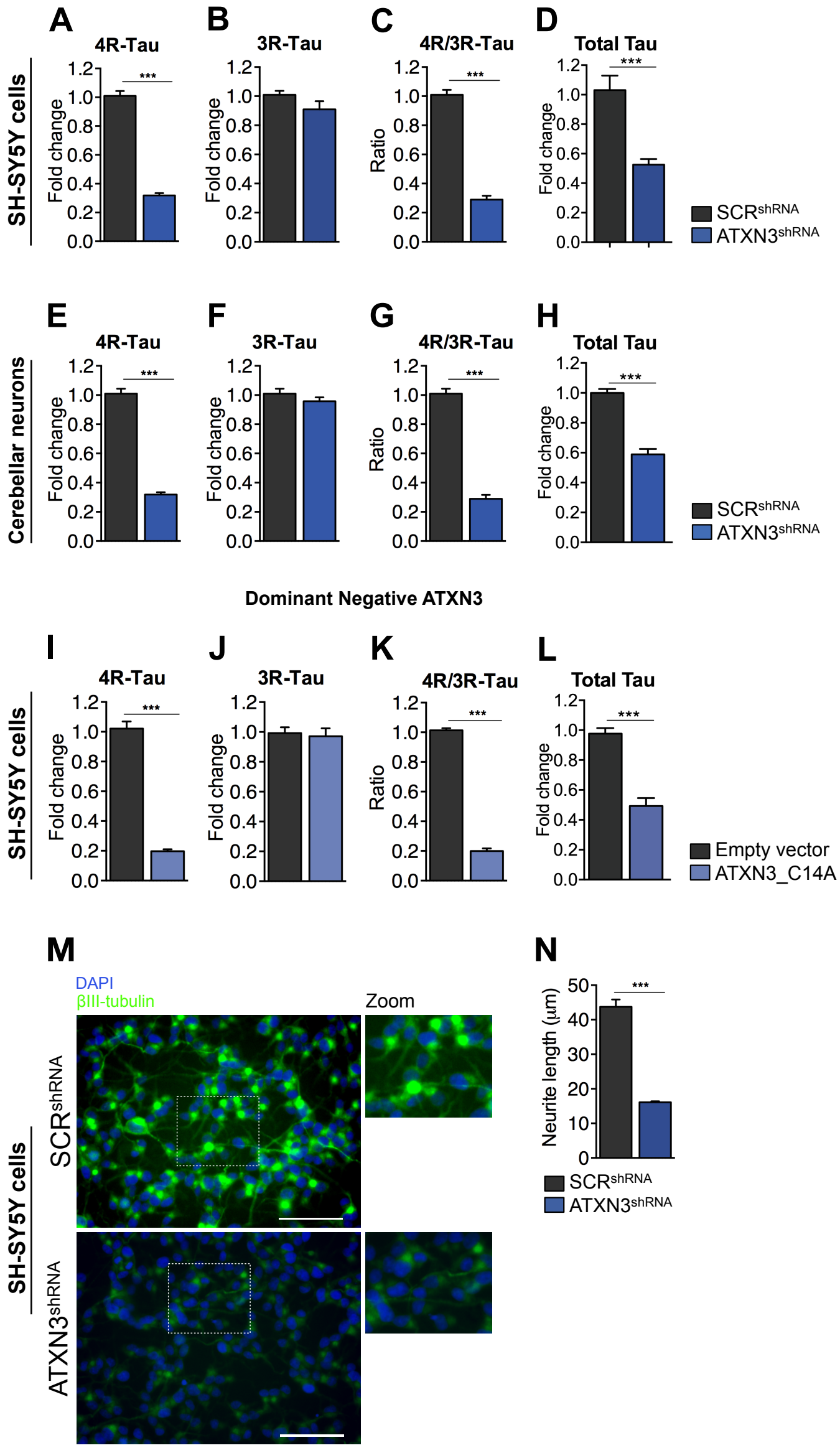
A
4R-Tau
B
3R-Tau
C
4R/3R-Tau
D
Total Tau
SH-SY5Y cells
Fold change
Ratio
***
SCRshRNA
ATXN3shRNA
E
F
G
H
Cerebellar neurons
Dominant Negative ATXN3
I
J
K
L
Empty vector
ATXN3_C14A
M
DAPI
βIII-tubulin
Zoom
SCRshRNA
ATXN3shRNA
N
Neurite length (μm)

Figure 5

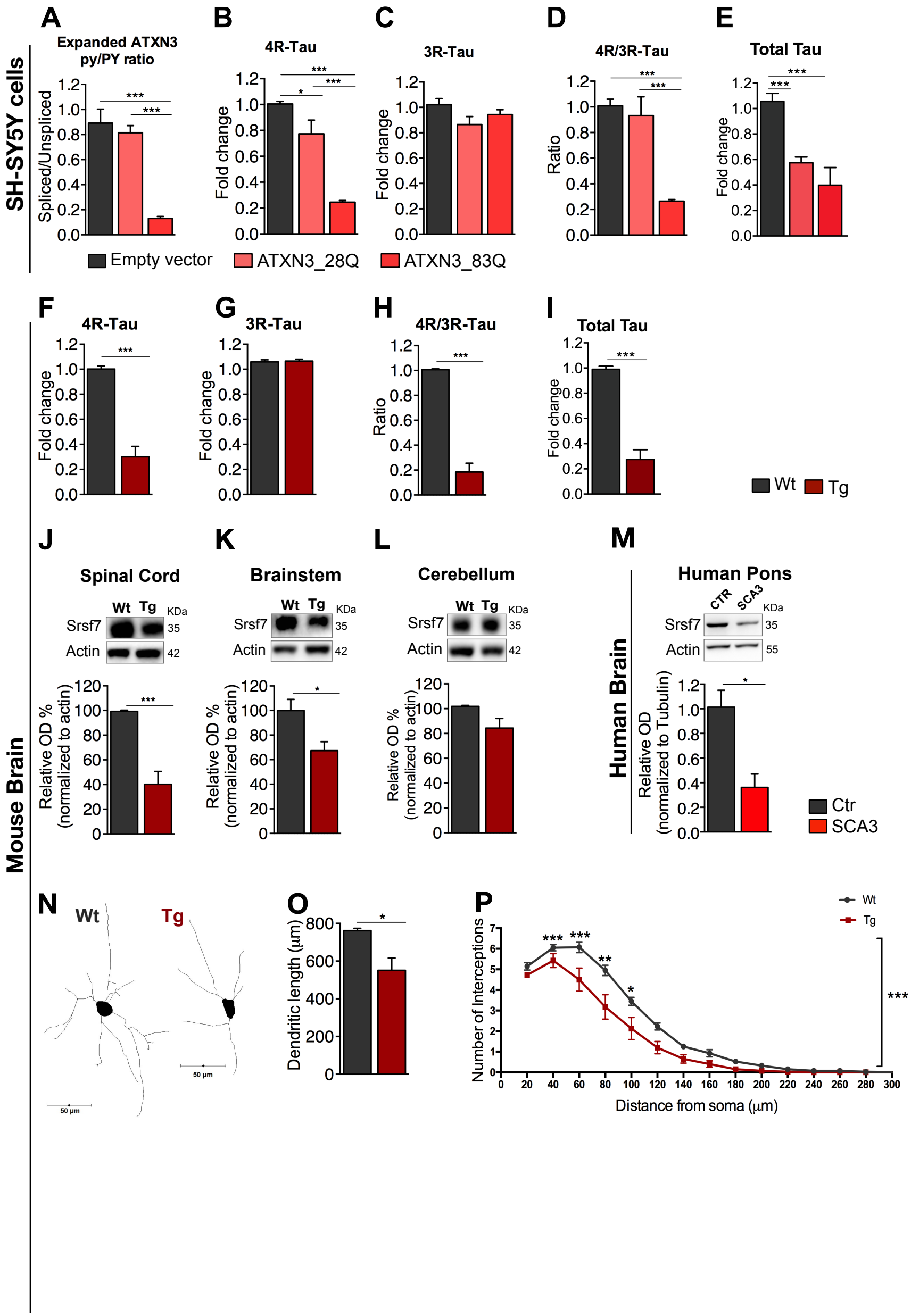
SH-SY5Y cells
A
Expanded ATXN3 py/PY ratio
Spliced/Unspliced
B
4R-Tau
Fold change
C
3R-Tau
Fold change
D
4R/3R-Tau
Ratio
E
Total Tau
Fold change
Empty vector
ATXN3_28Q
ATXN3_83Q
F
4R-Tau
Fold change
G
3R-Tau
Fold change
H
4R/3R-Tau
Ratio
I
Total Tau
Fold change
Wt
Tg
Mouse Brain
J
Spinal Cord
K
Brainstem
L
Cerebellum
Wt Tg KDa
Srsf7 35
Actin 42
Relative OD % (normalized to actin)
M
Human Pons
CTR SCA3 KDa
Srsf7 35
Actin 55
Human Brain
Relative OD (normalized to Tubulin)
Ctr
SCA3
N
Wt
Tg
50 µm
O
Dendritic length (µm)
P
Wt
Tg
Number of Interceptions
Distance from soma (µm)

Figure S1

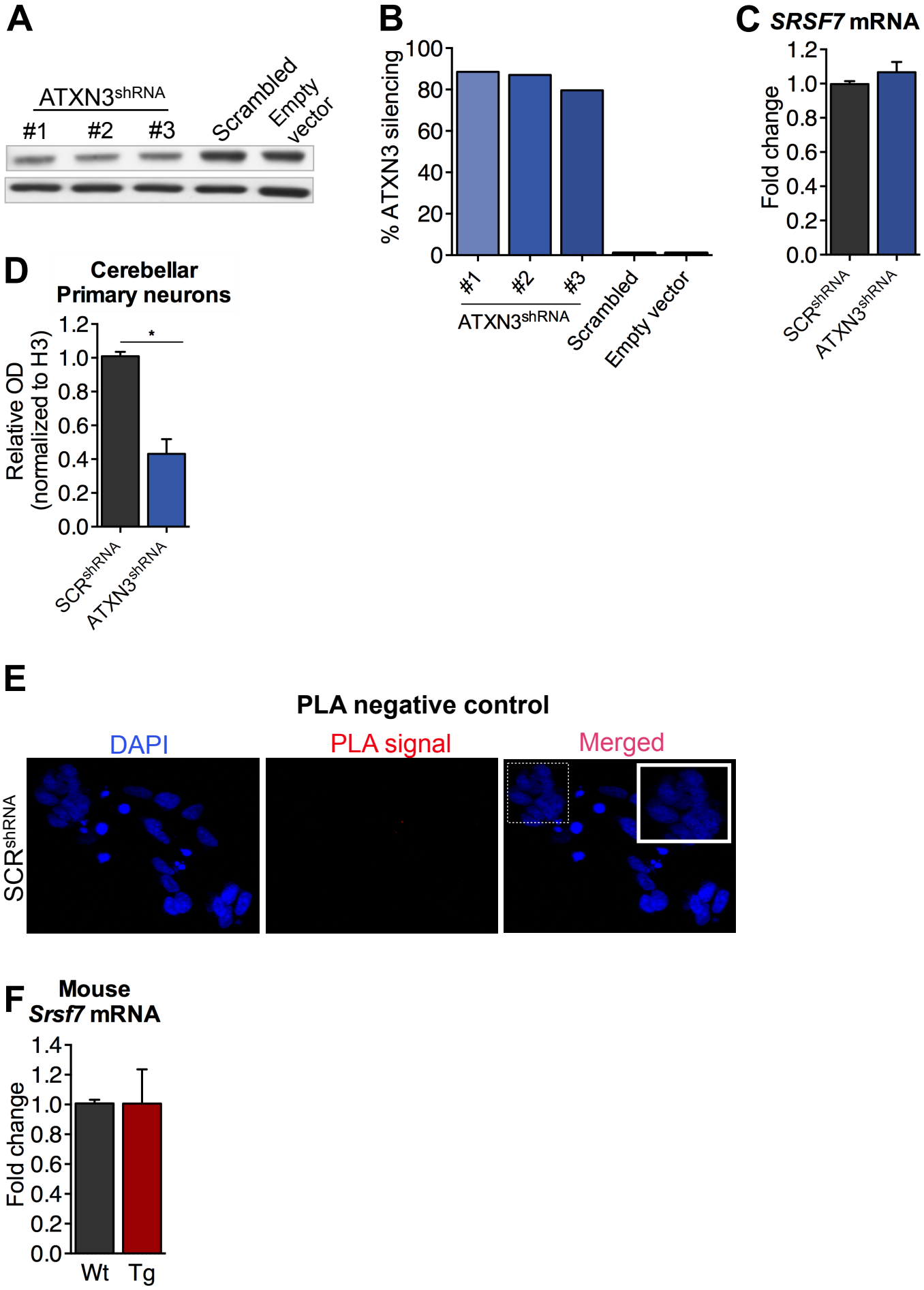
A
ATXN3shRNA
#1
#2
#3
Scrambled
Empty vector
B
% ATXN3 silencing
100
80
60
40
20
0
#1
#2
#3
ATXN3shRNA
Scrambled
Empty vector
C
SRSF7 mRNA
Fold change
1.2
1.0
0.8
0.6
0.4
0.2
0.0
SCRshRNA
ATXN3shRNA
D
Cerebellar Primary neurons
Relative OD (normalized to H3)
1.2
1.0
0.8
0.6
0.4
0.2
0.0
*
SCRshRNA
ATXN3shRNA
E
PLA negative control
DAPI
PLA signal
Merged
SCRshRNA
F
Mouse Srsf7 mRNA
Fold change
1.4
1.2
1.0
0.8
0.6
0.4
0.2
0.0
Wt
Tg